HHS Public Access

Author manuscript

Biol Cell. Author manuscript; available in PMC 2024 November 22.

Published in final edited form as:

Biol Cell. 2022 January ; 114(1): 3–31. doi:10.1111/boc.202100007.

Alpha-arrestins Aly1 and Aly2 regulate trafficking of the glycerophosphoinositol transporter Git1 and impact phospholipid homeostasis

Benjamin P. Robinson[b], **Sarah Hawbaker**[a], **Annette Chiang**[a], **Eric M. Jordahl**[a], **Sanket Anaokar**[b], **Alexiy Nikiforov**[b], **Ray W. Bowman II**[a,b], **Philip Ziegler**[b], **Ceara K. McAtee**[a], **Jana Patton-Vogt**[b], **Allyson F. O'Donnell**[a,b,*]

[a]Department of Biological Sciences, University of Pittsburgh, Pittsburgh, PA, USA.

[b]Department of Biological Sciences, Duquesne University, Pittsburgh, PA, USA.

Abstract

Phosphatidylinositol (PI) is an essential phospholipid, critical to membrane bilayers. The complete deacylation of PI by B-type phospholipases produces intracellular and extracellular glycerophosphoinositol (GPI). Extracellular GPI is transported into the cell via Git1, a member of the Major Facilitator Superfamily of transporters at the yeast plasma membrane. Internalized GPI is degraded to produce inositol, phosphate and glycerol, thereby contributing to these pools. *GIT1* gene expression is controlled by nutrient balance, with phosphate or inositol starvation increasing *GIT1* expression to stimulate GPI uptake. However, less is known about control of Git1 protein levels or localization. We find that the α-arrestins, an important class of protein trafficking adaptor, regulate Git1 localization and this is dependent upon their interaction with the ubiquitin ligase Rsp5. Specifically, α-arrestin Aly2 stimulates Git1 trafficking to the vacuole under basal conditions, but in response to GPI-treatment, either Aly1 or Aly2 promote Git1 vacuole trafficking. Cell surface retention of Git1, as occurs in *aly1*Δ *aly2*Δ cells, is linked to impaired growth in the presence of exogenous GPI and results in increased uptake of radiolabeled GPI, suggesting that accumulation of GPI somehow causes cellular toxicity. Regulation of α-arrestin Aly1 by the protein phosphatase calcineurin improves steady-state and substrate-induced trafficking of Git1, however, calcineurin plays a larger role in Git1 trafficking beyond regulation of α-arrestins. Finally, we find that loss of Aly1 and Aly2 leads to increased phosphatidylinositol-3-

*Corresponding author: Department of Biological Sciences, University of Pittsburgh, 4249 Fifth Avenue, Pittsburgh, PA, USA 15206, allyod@pitt.edu.

Author contributions

B.P.R. collected the majority of the data and wrote and revised the manuscript. S.H. wrote the automated quantification pipeline, ensured it functioned correctly, and trained users, as well as edited the manuscript. A.C. collected all data for the revision, the data on phospholipid localization and edited the manuscript. E.M.J. and C.K.M. performed data analysis and edited the manuscript. S.A, A.N, and P.Z. collected data on lipid uptake. R.W.B collected preliminary data for the manuscript, built several strains and reagents needed for the study and edited the manuscript. J.P.V. conceptualized the study and edited the manuscript. A.F.O. conceptualized the studies, performed the experiments, wrote and revised the manuscript.

Conflicts of interest statement

The authors have no competing or conflicting interests to declare.

Ethics approval and consent to participate

There are no experiments done in animal models in this work and no human subjects in the described work. The work presented herein represents original research, all authors have agreed to the content, and we will make the materials available to other researchers in a timely fashion upon their request.

phosphate on the limiting membrane of the vacuole, which is further exacerbated by GPI addition, suggesting that the effect is partially linked to Git1. Loss of Aly1 and Aly2 leads to increased incorporation of inositol label from [^{3}H]-inositol-labelled GPI into PI, confirming that internalized GPI influences PI balance and indicating a role for the α-arrestins in this regulation.

Keywords

E3 ubiquitin ligase; endocytosis; *S. cerevisiae* ; vacuole; calcineurin; microscopy; protein trafficking adaptors

Introduction

Eukaryotic membrane-bound organelles have unique lipid compositions that alter their function and influence protein trafficking to and from these compartments (Behnia and Munro, 2005; Strahl and Thorner, 2007; Klug and Daum, 2014; Casares et al., 2019). Imbalances in lipids, nucleotides or amino acids often result in cellular toxicity (Kim et al., 2000; Risinger et al., 2006; Ljungdahl and Daignan-Fornier, 2012; Shyu et al., 2019; Ruiz et al., 2020). Here we focus on regulation of the glycerophosphoinositol (GPI) transporter Git1 and consider how elevated cellular GPI, which increases phosphatidylinositol (PI), alters phospholipid homeostasis (Patton et al., 1995; Patton-Vogt and Henry, 1998).

In normal metabolism, PI is deacylated by B-type phospholipases to produce GPI (Angus and Lester, 1972; Patton et al., 1995). GPI, along with the complex inositol-containing sphingolipids, are the major products of PI turnover (Angus and Lester, 1972). GPI, and to a lesser extent, glycerophosphocholine, enters the cell via the Git1 transporter (Patton-Vogt and Henry, 1998; Fisher et al., 2005). Internalized GPI is converted to inositol, phosphate and glycerol, thus contributing to the cellular pools of these metabolites (Patton-Vogt and Henry, 1998). Git1 was first cloned for its ability to restore growth to the inositol auxotroph, *ino1*, (Patton-Vogt and Henry, 1998), demonstrating that GPI uptake via Git1 provides inositol to cells (Almaguer et al., 2003; Almaguer et al., 2004). Not surprisingly, transcription of *GIT1* is regulated by inositol, and more exquisitely by phosphate (Almaguer et al., 2003; Almaguer et al., 2004). The *GIT1* promoter contains binding sites for Pho2 and Pho4 (Almaguer et al., 2004), transcription factors that respond to phosphate limitation by cooperatively binding to genes needed for phosphate uptake and/or scavenging (Vogel et al., 1989; Magbanua et al., 1997; Shao et al., 1998). The *GIT1* promoter further contains inositol and choline responsive elements (ICREs) for the heteromeric Ino2/Ino4 transcription factors, which stimulate *GIT1* expression during inositol starvation.

Once GPI enters the cell through Git1, released free inositol fluxes into PI, which in turn is a precursor to two important classes of lipids: polyphosphoinositides and sphingolipids (Figure 1A) (Angus and Lester, 1972; Patton et al., 1995). Phosphoinositides are an important but minor class of membrane lipids produced by phosphorylation/dephosphorylation of carbons 3, 4 and 5 in the inositol ring of PI. Each organelle and/or subdomain is enriched for a specific class of phosphorylated PI (Di Paolo and De Camilli, 2006; Strahl and Thorner, 2007). Phospholipids are important binding sites on membranes that regulate trafficking and signaling events. In contrast, sphingolipids are a major lipid

species with roles endocytosis, actin organization, response to heat stress, calcium sensitivity and cell cycle regulation (Klemm et al., 2009; Epstein et al., 2012; Klug and Daum, 2014; Montefusco et al., 2014). PI is used in *de novo* sphingolipid synthesis at two steps in the complex sphingolipid base formation (see Figure 8C) (Dickson et al., 2006; Klug and Daum, 2014; Montefusco et al., 2014); perturbations in PI alter sphingolipid synthesis, with increasing PI favoring elevated sphingolipid biosynthesis (Henry et al., 2012).

GPI transport via Git1 impacts PI synthesis and downstream biosynthetic pathways, making it critical to define the factors that govern this protein's stability and/or trafficking. Git1 is a 12-pass transmembrane domain protein that functions at the PM and is a member of the Major Facilitator Superfamily (MFS) (Mariggio et al., 2006). It contains sugar transporter-like domains, suggestive of a shared structural relationship to the glucose transporters in *Saccharomyces cerevisiae*. While there is no clear mammalian ortholog of Git1, mammalian glucose transporter Glut2 can uptake GPI and is considered functionally analogous (Mariggio et al., 2006). The trafficking of the other transporters needed for inositol uptake, such as Itr1 and Itr2, and members of the related glucose transporter family, including Hxt1, Hxt3, and Hxt6, are controlled by the α-arrestins, a family of protein trafficking adaptors (Nikko and Pelham, 2009; Harada et al., 2010; O'Donnell et al., 2015; Hovsepian et al., 2017; Ivashov et al., 2020). We sought to determine if the α-arrestins might similarly regulate Git1 trafficking, whose removal from the cell surface was previously linked to clathrin-mediated endocytosis (Almaguer et al., 2006).

The α-arrestins, conserved from yeast to man, act as bridges between membrane proteins (referred to as cargos) and Rsp5, a ubiquitin ligase that regulates the endocytosis of several nutrient permeases (Rotin and Kumar, 2009). Internalization of many nutrient transporters is induced by excess substrate and their ubiquitination by Rsp5 facilitates their interaction with the endocytic machinery (Blondel et al., 2004; Lin et al., 2008; Nikko and Pelham, 2009; Ivashov et al., 2020). Modification of cargos by even a single ubiquitin is often sufficient to induce internalization (Shih et al., 2000; Raiborg et al., 2002; Stringer and Piper, 2011). However, many cargos lack the motifs to directly recruit Rsp5. Instead, the α-arrestins selectively bind to membrane cargos and simultaneously interact with the WW-domains of Rsp5 via their PPxY motifs (Gupta et al., 2007; Lin et al., 2008; Nikko et al., 2008; Becuwe et al., 2012; O'Donnell et al., 2013; Alvaro et al., 2014). Thus, α-arrestins link membrane cargo to the machinery needed for selective endocytosis of an expanding array of membrane proteins (reviewed in this issue of Biology of the Cell (Kahlhofer et al., 2020)).

Relevant to our studies, α-arrestin Art5 controls inositol influx by regulating the inositol-stimulated endocytosis of inositol transporter Itr1, and perhaps Itr2 (Nikko and Pelham, 2009; Yamagami et al., 2015). Alterations in cellular inositol balance, as occurs in response to mis-regulation of Itr1, have broad reaching implications in the cell, including causing changes to mitochondrial cardiolipin production by altering CDP-diacylglycerol levels (Harada et al., 2010; Tamura et al., 2013) and restoring polarized trafficking to cells where phospholipid flippases are mutated (Yamagami et al., 2015). Thus, ties between inositol balance, phospholipids and α-arrestins are established.

Here we add new players in regulating GPI and inositol in cells; We show that the paralogous *arrestin-like yeast proteins 1* and *2* (Aly1 and Aly2) act as adaptors for Git1. This is a novel membrane protein cargo for these α-arrestins, which regulate the trafficking three amino acid permeases, a G-protein coupled receptor, an arsenite transporter, and a P-type ATPase (Hatakeyama et al., 2010; O'Donnell et al., 2010; O'Donnell et al., 2013; Crapeau et al., 2014; Hager et al., 2018; Wawrzycka et al., 2019; Nishimura et al., 2020; Sen et al., 2020). Only a handful of transporters are linked to the Alys to date, but the diversity of cargos regulated by this family is rapidly expanding (Savocco et al., 2019). In this study, we show that α-arrestins operate in basal, unstimulated conditions to control the steady-state turnover of Git1 and are induced to internalize Git1 in the presence of GPI. Excessive uptake of GPI is toxic, though the mechanism of this toxicity remains unclear. Consistent with earlier studies, we find that Git1 is regulated in part by the clathrin-mediated endocytic pathway (Almaguer et al., 2006); however, an intracellular sorting pathway also controls Git1 since endocytic blocks do not fully recapitulate the defective trafficking observed with loss of the Alys.

While Aly1 and Aly2 share functional similarities, Aly2 plays a dominant role in trafficking Git1, which is especially evident in basal turnover of Git1. Interestingly, while α-arrestin Aly1 is regulated by the protein phosphatase calcineurin (CN) (O'Donnell et al., 2013), however we found only modest contributions for this pathway in Git1 steady-state trafficking. When we explored GPI substrate-induced phenotypes we found that a phosphomimetic allele of Aly1 failed to rescue *aly1*Δ *aly2*Δ sensitivity to GPI and the mutant allele that mimicked the dephosphorylated state of Aly1 was better able to control GPI-induced Git1 internalization. Thus, CN appears to play a role in Aly1-mediated, substrate-induced trafficking of Git1.

Finally, loss of the Alys results in a sharp shift in phosphatidyl-inositol-3-phosphate (PI(3)P) balance in the endomembrane system, with a dramatic increase in PI(3)P levels in the limiting membrane of the vacuole (Schu et al., 1993; Burd and Emr, 1998; Gillooly et al., 2000). This alteration in PI(3)P does not appear to reflect an overall alteration of PIPs as other phosphoinositides are largely unchanged in the absence of the Alys. While uptake of GPI exacerbates this defect, leading to more PI(3)P on the vacuolar membrane in both wild-type and *aly1*Δ *aly2*Δ cells, it is unlikely that this change in PI(3)P abundance in *aly1*Δ *aly2*Δ is entirely due to GPI uptake via Git1. However, we confirm that [^{3}H]-inositol derived from exogenously supplied [^{3}H]-inositol-GPI is incorporated into PI (Patton et al., 1995; Patton-Vogt and Henry, 1998), the precursor to both the inositol-containing complex sphingolipids and PIPs and that label incorporation into PI increases in the absence of Aly and Aly2. Overall, we find that the α-arrestins Aly1 and Aly2 are new regulators of GPI uptake via Git1 and, thereby, impact cellular PI levels and downstream lipid species.

Results

Trafficking of Git1 is impaired in the absence of α-arrestins Aly1 and Aly2

We sought to determine if the α-arrestins control Git1 localization. To avoid confounding issues caused by endogenous *GIT1* gene expression, we expressed Git1-GFP from the constitutive *TEF1* promoter and examined growth of cells lacking 9 of the 14 yeast α-

arrestins (referred to as 9ArrΔ (Nikko and Pelham, 2009)) on medium with Git1's substrate, GPI. The 9ArrΔ cells were exquisitely sensitive to growth on medium containing GPI, while wild-type cells grew well at the concentrations of GPI employed (Figure 1B). Functional complementation assays with plasmids expressing each of the missing α-arrestins in the 9ArrΔ cells showed that the paralogous α-arrestins Aly1 or Aly2 restored growth of 9ArrΔ cells on GPI. The 9ArrΔ cells' sensitivity to GPI might arise due to excessive GPI uptake, which be caused by increased Git1 activity or abundance at the PM, and/or imbalance of downstream metabolites (Figure 1A). We assessed Git1-GFP steady-state localization using confocal microscopy. Consistent with potentially elevated GPI import in the 9ArrΔ cells, Git1 was retained at the PM while in wild-type cells Git1 localized faintly to the PM with substantial vacuole fluorescence (Figure 1C). Git1 at the PM in 9ArrΔ cells was reduced in cells expressing *ALY2* and the PM/vacuole fluorescence ratio in cells expressing either *ALY1* or *ALY2* was significantly reduced, demonstrating augmented Git1-GFP trafficking to the vacuole (Figures 1C-D and Suppl. Fig 1A). However, plasmids expressing the other α-arrestins failed to improve growth on GPI or reduce the retention of Git1 at the cell surface (Figures 1B-C and Suppl Fig. 1A). Manual quantification of the PM and vacuolar fluorescence intensities for Git1-GFP supported these conclusions, showing significantly reduced PM/vacuole fluorescence ratios in wild-type cells compared to the 9ArrΔ cells (Figure 1D). Addition of either Aly1 or Aly2 significantly reduced the PM/vacuole ratio of 9ArrΔ cells, with Aly2 having the more robust effect (Figure 1D), however only Aly2 significantly reduced the PM fluorescence of Git1-GFP (Suppl. Fig. 1A), suggesting that over this time-course of exposure to GPI (2h treatment) Aly2 is more effective than Aly1 at reducing the surface pool of Git1-GFP. However, over the longer-time course of a growth assay on GPI (as in Figure 1B), Aly1 may also reduce the surface abundance Git1-GFP, thereby accounting for this altered sensitivity. The other α-arrestins did not significantly reduce the PM alone or PM/vacuole fluorescence ratio (Figure 1D and Suppl. Fig 1A), yet some did increase the PM/vacuole ratio (Art10 and Art5) based on the manual quantification only. This difference between the manual and automated quantification may reflect the ability of the automated quantification to capture outliers in comparison with manual quantification.

Our lab has made extensive use of manual fluorescence quantification (O'Donnell et al., 2015; Prosser et al., 2015; Chandrashekarappa et al., 2016; Hager et al., 2018; Soncini et al., 2020) and the process is a time consuming and limiting factor for analyses; For manual quantification, we typically quantify ~100 cells with at least two full imaging fields being measured (O'Donnell et al., 2015). To facilitate this kind of quantification, we developed an automated pipeline using an R-script program we wrote called '*CellQuant*' (see Materials and Methods; script available at www.odonelllab.com and on Github at https://github.com/sah129/CellQuant). We re-ran our analyses to measure the PM and vacuolar fluorescence intensity for the images in Figure 1C using this automated pipeline and had strong agreement with our manual data set. The time taken to obtain this quantification was a fraction of that needed for the manual quantification (~30 mins compared to >20 hours) (Figure 1E). The imaging data, quantification, and GPI growth assays were consistent with the results of Git1-GFP immunoblot analyses, where we found less full-length Git1-GFP in protein extracts from wild-type cells than in those from 9ArrΔ cells. In wild-type cells

significant signal was observed for the free GFP-breakdown product, often associated with cleaved GFP in the vacuole after degradation of GFP-tagged transporters (Li et al., 1999; Nikko and Pelham, 2009), while in the 9ArrΔ cells there was very little GFP-breakdown product (Figure 1F). Addition of Aly1 or Aly2 to 9ArrΔ cells increased the free GFP-breakdown product abundance and reduced the Git1-GFP abundance, thereby elevating the ratio of free GFP/Git1-GFP (Figure 1F). Expression of the other α-arrestins in the 9ArrΔ cells had modest effects on total Git1-GFP levels and did very little to increase the abundance of the GFP-breakdown product, however Art1 and Csr2 elevated the GFP/Git1-GFP ratio above the vector control and in other replicates we saw elevated GFP/Git1-GFP ratios for Art10 (Figure 1F, data not shown). Taken together these data show that the α-arrestins Aly1 and Aly2 help traffic Git1 to the vacuole for degradation, either by stimulating its endocytosis or its intracellular sorting from the Golgi and/or endosomes to the vacuole. We do not exclude the possibility that other α-arrestins may play added roles in Git1 trafficking; indeed many α-arrestins often regulate a single transporter under disparate conditions (Nikko and Pelham, 2009) and the elevated free GFP breakdown product suggests that some of them are at least partially operational with Git1. Additionally, these findings show that our new automated quantification pipeline is effective for measuring PM and vacuole fluorescence abundance, and we will assess its utility throughout this paper.

To this point our analyses hinged on the 9ArrΔ cells, however this background is missing only 9 of the 14 yeast α-arrestins. Given the data indicating that addition of some of the α-arrestins to 9ArrΔ cells resulted in increased PM retention of Git1, we sought to determine if the other α-arrestins that are intact in 9ArrΔ cells might contribute to Git1 trafficking. A recent paper demonstrated that the α-arrestins and other adaptors that bind the ubiquitin ligase Rsp5 may compete for a limited pool of Rsp5 and therefore restrict its function (MacDonald et al., 2020). We observed that when α-arrestins other than Aly1 or Aly2 were expressed in the 9ArrΔ background there may be elevated Git1 PM/vacuole ratios (Figure 1D), a result that might be obtained if the expression of an α-arrestin unable to traffic Git1 interfered with the activity of the remaining endogenous α-arrestin. The 9ArrΔ cells retain 5 other α-arrestins, including Bul1 and Bul2, which have overlapping functions in other Aly1/Aly2-mediated trafficking events (Novoselova et al., 2012; Crapeau et al., 2014). We next determined if the Buls influence Git1 trafficking. GPI growth assays showed only a slight change in sensitivity for *bul1*Δ *bul2*Δ cells relative to wild-type cells (Suppl. Figure 2A). Deletions of *ALY1 ALY2* and *BUL2* showed similar sensitivities to GPI as the *aly1*Δ *aly2*Δ cells, though the *aly1*Δ *aly2*Δ *bul1*Δ cells displayed a bit more resistance to GPI than *aly1*Δ *aly2*Δ (Suppl. Figure 2A). These data suggest that the Buls may play a role in Git1 trafficking. Furthermore, imaging of Git1 in the absence of Buls showed greatly reduced Git1 at the PM in all cells lacking any combination of Buls (Suppl. Figure 1B-D). Perhaps this is due to increased protein degradation/turnover in the absence of these α-arrestins, which has been reported previously (Savocco et al., 2019) and could be due to a lack of competition by remaining α-arrestins for the Rsp5 ubiquitin ligase. Alternatively, the Bul proteins may influence expression from the *TEF1* promoter used for *GIT1* in these experiments, though most effects of α-arrestins described to date have been post-transcriptional in nature. Interestingly, while the loss of *bul1*Δ *bul2*Δ caused mild sensitivity to GPI and *bul1*Δ or *bul2*Δ alone did not alter the GPI sensitivity, each

of these mutants reduced the PM abundance of Git1-GFP fluorescence (Suppl. Figure 2B-D), indicating an added unknown secondary cause for sensitivity to GPI in these *bul*Δ backgrounds that is not strictly linked to the abundance of Git1-GFP at the cell surface. Given the complex results with these mutants, the contributions of Buls to Git1 trafficking will be explored in more detail elsewhere but these findings highlight the fact that GPI sensitivity cannot simply be correlated to Git1 retention at the cell surface. Perhaps there are elements that alter the activity of the transporter at the PM; Git1 is a protein symporter and elevated pH has been shown to decrease Git1 activity (Almaguer et al., 2004) but beyond this nothing is known about Git1 activity regulation. From here on we focus our experimental attention on the roles of Aly1 and Aly2.

To further confirm that Aly1 and Aly2 are important for Git1 regulation, we assessed the sensitivity of *aly1*Δ *aly2*Δ cells to GPI in comparison to wild-type and 9ArrΔ cells. We found that loss of either *ALY1* or *ALY2* sensitized cells to GPI, with loss of *ALY2* causing the more severe inhibition (Figure 2A). Cells lacking both *ALY1* and *ALY2* were more sensitive to GPI than either single mutant and had the same degree of GPI sensitivity as the 9ArrΔ cells (Figure 2A). Fluorescent imaging of Git1-GFP in *aly1*Δ *aly2*Δ cells revealed Git1 retention at the PM (Suppl. Figure 1B) and significantly increased PM/vacuole ratio in these cells that is comparable to that of 9ArrΔ, as judged by both our manual and automated quantification pipelines (Figures 2B-D). Loss of *ALY2* alone increased Git1-GFP at the PM, while deletion of *ALY1* had no significant impact, suggesting that under these steady-state conditions Aly1 has a modest impact on Git1 trafficking (Figures 2B-D and Suppl. Figure 1B). Protein extracts from *aly2*Δ or *aly1*Δ *aly2*Δ cells revealed little difference in Git1-GFP abundance between them but both strains had less free GFP than the *aly1*Δ or wild-type cells and an overall reduction in the GFP/Git1-GFP ratio that was comparable to that of 9ArrΔ cells (Figure 2E). However, in 9ArrΔ cells the Git1-GFP was more abundant than in *aly1*Δ *aly2*Δ cells (Figures 2B-E) suggesting some contribution by the other α-arrestins or Bsd2, an Rsp5 adaptor operating in the Golgi, to Git1 trafficking under these conditions (as also indicated by Figure 1).

To confirm that the plasmid-borne, GFP-tagged version of Git1 was functional and accurately reflected events that regulate endogenous Git1, we performed short-term radiolabeled GPI transport assays (5 min) in wild-type and *aly1*Δ *aly2*Δ cells with and without the Git1-GFP plasmid. These cells were grown in high phosphate medium, where expression of Git1 would be at basal levels and not induced as it would be under phosphate or inositol starvation conditions (Almaguer et al., 2003). Even under these high phosphate conditions, we found that loss of α-arrestins *ALY1* and *ALY2* increased the rate of GPI transport into cells by more than ~3-fold compared to wild-type cells (Figure 2F). To ensure that the Git1-GFP construct was functional, we also assessed radiolabeled GPI uptake in wild-type or *aly1*Δ *aly2*Δ cells harboring the Git1-GFP plasmid. In cells expressing Git1-GFP from a constitutive promoter, GPI uptake was increased by ~100-fold in wild-type cells grown in high phosphate medium (compare Figures 2F and 2G). Cells lacking *ALY1* and *ALY2* nearly doubled this rate of uptake (Figure 2G), again consistent with retention and/or elevated activity of Git1 at the cell surface in the absence of these α-arrestins. In addition to these uptake assays, we examined the ability of the Git1-GFP plasmid to rescue growth of *git1*Δ on medium lacking phosphate and containing GPI. Earlier studies found that cells can

grow when supplemented with GPI as the sole phosphate source (Almaguer et al., 2004). Growth on media containing GPI the sole phosphate source was rescued to wild-type levels in *git1*Δ cells expressing the Git1-GFP plasmid (Suppl. Figure 3A). These data demonstrate that the GFP-tagged Git1 is functional, allowing GPI to be used as a phosphate source. In limiting phosphate conditions Git1-GFP expression in *aly1*Δ *aly2*Δ cells is not toxic, perhaps because it is used as an added phosphate source here (Suppl. Figure 3A).

To more carefully assess regulation of endogenous Git1, we made a chromosomally integrated, GFP-tagged version of this gene under its own promoter. We then examined Git1-GFP localization in cells grown in medium that contained high or low levels of phosphate, with or without inositol. Expression of Git1 is upregulated in response to phosphate and inositol limitation by the Pho2/Pho4 and Ino2/Ino4 transcription factors (Almaguer et al., 2003). As expected, regardless of the inositol content, in high phosphate medium there was little to no detectable Git1 by fluorescence microscopy (Figures 3A-B, note that 9ArrΔ cells in these conditions were sick and faint GFP fluorescence observed was due to a dead cell). When cells were incubated in low phosphate medium Git1-GFP fluorescence was observed (Figures 3C-D). Under low phosphate conditions, the wild-type cells had predominantly vacuolar GFP fluorescence, yet *aly1*Δ *aly2*Δ or the 9ArrΔ cells retained Git1-GFP at the PM. Of note, there was reduced vacuole fluorescence in 9ArrΔ cells compared to *aly1*Δ *aly2*Δ cells, indicating that other α-arrestins or Bsd2 are involved in the Git1 trafficking. The fluorescence intensity for each of these was slightly brighter when cells were additionally incubated in medium without inositol, consistent with the earlier studies of *GIT1* expression (Almaguer et al., 2003). Manual quantification of this data found a substantially brighter PM/vacuole fluorescence ratio in the *aly1*Δ *aly2*Δ and 9*Arr*Δ cells in low phosphate medium with or without inositol (Figures 3E-F) and that 9ArrΔ is higher still than the *aly1*Δ *aly2*Δ cells. We performed automated quantification of these data but used a slightly different algorithm that used the DIC channel to define the cell surface since the PM fluorescence for the wild-type cells was too low and difficult to capture via our standard approach (see Methods). These data agree with our manual quantification, although there was some compaction in the range of values identified in the automated quantification (Suppl. Figures 3B-C). Taken together, these findings are consistent with our observations that the α-arrestins, in particular Aly1 and Aly2, contribute to Git1 trafficking and their absence results in increased levels of Git1 at the cell surface. However, there must also be other α-arrestins able to contribute to Git1 trafficking as the defect in the 9ArrΔ cells was more severe than that observed in *aly1*Δ *aly2*Δ alone.

We further explored the role of Aly1 and Aly2 in regulating Git1 function under shifting phosphate conditions using short-term GPI transport assays (Surlow et al., 2014). When wild-type cells were shifted from high to low phosphate medium to induce Git1 expression, GPI transport increased ~14-fold (Figure 3G). In *aly1*Δ *aly2*Δ cells grown in low phosphate medium, the GPI transport rate was ~3-fold higher than that of wild-type cells in low phosphate or *aly1*Δ *aly2*Δ cells in high phosphate medium (Figure 3G). Together, these data demonstrate that the loss of *ALY1* and *ALY2* increases GPI uptake by endogenous, untagged Git1 in response to phosphate starvation and are consistent with our findings that Git1-GFP is retained at the cell surface in *aly1*Δ *aly2*Δ cells (Figures 2B-E, 3C-F and Suppl. Figure 3B-C).

Git1 internalization is induced by GPI and is dependent upon α-arrestins Aly1 and Aly2

Our experiments to this point indicate that Aly1 and Aly2 play a role in the steady-state internalization and/or trafficking to the vacuole of Git1, with Aly2 performing most of this trafficking and Aly1 only altering Git1 localization when added to the 9ArrΔ cells (Figure 1B-F). For many transporters, addition of their substrate triggers conformational changes that stimulate their vacuolar sorting and/or endocytic turnover (Gournas et al., 2010; Keener and Babst, 2013; Ghaddar et al., 2014; Gournas et al., 2017). We monitored Git1-GFP in response to GPI addition in wild-type cells treated with GPI and found that Git1 fluorescence at the PM was reduced and fluorescence shifted to the lumen of the vacuole in wild-type cells after GPI addition (Figures 4A-B). We examined Git1-GFP breakdown post GPI addition via immunoblotting and found that in WT cells the GFP/Git1-GFP ratio was much higher, but in *aly1*Δ *aly2*Δ or 9ArrΔ cells the ratio only increased slightly or not at all (Figure 4C). More detailed analysis of Git1 localization in response to GPI in WT or *aly1*Δ *aly2*Δ cells containing vector or Aly1 or Aly2 complementing plasmids showed that the GPI-induced shift in Git1 localization was largely lost in *aly1*Δ *aly2*Δ cells (Figure 4D-E and Suppl. Figure 4A). Though some modest reduction in PM/vacuole ratio is observed at 2h post GPI addition, suggesting a GPI-induced and Aly1/Aly2-independent mechanism of reducing Git1 abundance during the 2-hour GPI exposure (Figures 4A-C). This idea is confirmed in the immunoblots where a slight reduction in Git1-GFP is also seen post GPI addition in *aly1*Δ *aly2*Δ or 9ArrΔ extracts (Figure 4C), again consistent with an α-arrestin independent regulation of Git1. Plasmid-borne Aly1 in *aly1*Δ *aly2*Δ cells increased Git1-trafficking to the vacuole upon GPI addition (Figures 4D-E and Suppl. Figure 4A compare 60 min treatment between Aly1 vs vector control). Interestingly, the ratio of PM/vacuole intensity in *aly1*Δ *aly2*Δ cells is initially still significantly higher than in wild-type cells when Aly1 was present, consistent with our earlier data showing that Aly1 plays a minor role in Git1 steady-state trafficking to the vacuole (Figures 4D-E and Figure 2). Addition of Aly2 to *aly1*Δ *aly2*Δ cells restored basal trafficking of Git1 to the vacuole, as indicated by the reduced PM/vacuole fluorescence ratios observed prior to GPI addition, which was not significantly different from the PM/vacuole ratios in wild-type cells (Figures 4D-E and Suppl. Figure 4A). However, GPI-induced trafficking was not as impacted by Aly2, with only modest drops in the PM/vacuole ratios at 60- and 120-mins post GPI addition, similar to what was observed for *aly1*Δ *aly2*Δ cells with just a vector control. Importantly, our manual and automated quantification of this imaging (Figures 4E and Suppl. Figure 4A, respectively) are consistent with one another. Taken together, these data support a model whereby Aly1 may play a more prominent role in the GPI-induced trafficking of Git1, while Aly2 is very effective at stimulating steady-state trafficking of Git1 to the vacuole. As borne out in earlier experiments, other factors also alter the localization of Git1 in response to GPI as even in the *aly1*Δ *aly2*Δ cells there was a significant reduction in the PM/vacuole fluorescence post GPI addition (Figure 4D-E, see 120 min timepoint for *aly1*Δ *aly2*Δ with vector). Perhaps this could be ascribed to Bul1/Bul2 function or another trafficking adaptor that can operate in this GPI-stimulated turnover pathway when the *ALY*s are deleted. Immunoblot analyses of Git1-GFP in *aly1*Δ *aly2*Δ cells containing vector, Aly1 or Aly2 plasmids and treated with GPI support the imaging data, demonstrating increased GFP/Git1-GFP ratios post GPI addition when Aly1 or Aly2 are present in these cells (Figure 4F).

To begin to define the relative contributions of endocytic trafficking versus intracellular sorting on Git1 accumulation in the vacuole under basal conditions and post GPI addition, we examined the Git1-GFP localization and GPI sensitivity of mutant cells lacking endocytic components. Consistent with our earlier findings, loss of *ALY1* and *ALY2* resulted in exquisite sensitivity to GPI and increased PM/vacuole ratios for Git1-GFP fluorescence (Figures 5A-C and 2A-C). Loss of the endocytic factor *END3*, which encodes an early arriving component of clathrin-mediated endocytic patches, similarly caused sensitivity to GPI and increased PM/vacuole fluorescence compared to wild-type (Figures 5A-C). Interestingly, deletion of *APL3* or *APL1*, which encode the α- and β-adaptin, respectively, of clathrin-associated protein complex 2 (AP-2), each gave rise to increased sensitivity to GPI, with *apl1*Δ cells having a more severe phenotype than *apl3*Δ cells (Figure 5A). While the role of AP-2 cargo selection for clathrin-mediated endocytosis is well-documented in mammals, in yeast this complex is only associated with the internalization of a few membrane proteins, though it clearly associates with early endocytic patches (Carroll et al., 2009; Carroll et al., 2012). We examined AP-2 in these studies because Aly1 and Aly2 physically interact with these adaptins (O'Donnell et al., 2010). Loss of *APL1* led to increased PM/vacuole ratios, while *apl3*Δ significantly impaired vacuolar trafficking of Git1, but not as robustly as *apl1*Δ (Figures 5B-C). Interestingly, none of these endocytic factors (*end3*Δ, *apl1*Δ or *apl3*Δ) increased the PM/vacuole ratio as much as loss of the *ALY*s (Figure 5B-C). Based on these data, we posit that some steady-state vacuolar trafficking of Git1 occurs via endocytosis, as vacuole-localized fluorescence diminishes in the endocytic mutants. Yet it appears that the *aly1*Δ *aly2*Δ cells additionally impair intracellular sorting of Git1. These data further suggest that AP-2 may play a role in regulating Git1 endocytosis.

To examine substrate-induced internalization and intracellular trafficking, we next examined the localization of Git1-GFP in cells treated with GPI that had either been preincubated in latrunculin A (LatA), which prevents actin polymerization to selectively block endocytosis while leaving intracellular sorting intact (Ayscough et al., 1997), or its vehicle control DMSO. Wild-type cells treated with LatA retained higher PM/vacuole fluorescence ratios after GPI addition (Figure 5D-E). However, the ratio was still significantly higher than the DMSO-treated cells after 2h of GPI, indicating that some of the trafficking to the vacuole was likely due to endocytosis while a portion of the trafficking was independent of this LatA-blocked pathway. Interestingly, the LatA-treated cells were not statistically different from the DMSO-treated cells prior to GPI addition, suggesting an intracellular sorting route for Git1 (Figure 5D-E). In *aly1*Δ *aly2*Δ cells treated this way, GPI induced a small amount of Git1-GFP trafficking to the vacuole (as measured by decreased PM/vacuole fluorescence ratio) and Aly1 addition reduced this ratio further but the effect was muted in the LatA-treated cells (Suppl. Figure 4B-C). In cells expressing Aly2 only, there was no impact of adding GPI to LatA-pretreated cells (Suppl. Figure 4B-C). Thus, although GPI induces endocytosis of Git1 and this accounts for a portion of the decreased PM/vacuolar ratio observed, the persistent decrease in the PM/vacuole ratio observed in LatA-treated cells after GPI addition suggests that there is a contribution of intracellular sorting to the vacuole for Git1-GFP in GPI-treated cells. Aly1 appeared better able to stimulate this intracellular sorting, as LatA-treated Aly1-expressing cells significantly dropped the PM/vacuole ratios

after GPI treatment. In contrast, Aly2 did not seem to operate in this pathway as cells expressing Aly2 failed to reduce PM/vacuole ratios after LatA and GPI treatments.

To further assess this regulation, we next treated endocytic mutants with GPI and monitored PM/vacuole fluorescence. Cells lacking the *ALY*s have reduced PM/vacuole ratio post GPI addition and GPI significantly reduced the PM/vacuole ratio in *end3*Δ, *vrp1*Δ and *apl1*Δ cells (Figure 5F-G and Suppl. Figure 4B-C). Note that we included Vrp1, which encodes the yeast form of the actin nucleator verprolin, in these studies as an orthogonal approach to using the *end3*Δ cells as these were very sick upon GPI addition. This persistent reduction in PM/vacuole ratios post GPI addition in LatA-treated or endocytic mutant strains suggests that either a clathrin-independent endocytic (Prosser et al., 2015) and/or intracellular sorting route exists to shuttle Git1-GFP to the vacuole post GPI addition. Since LatA prevents both clathrin-mediated and -independent endocytosis the persistent internalization of Git1 observed in LatA-treated cells suggests that the intracellular sorting function is more likely.

α-Arrestins Aly1 and Aly2 must interact with Rsp5 to regulate Git1 trafficking

α-Arrestins contain $^{L}/_{P}$PxY motifs which allow for association with WW-domain-containing proteins. In yeast, each of the α-arrestins has been shown to use these $^{L}/_{P}$PxY motifs to engage the ubiquitin ligase Rsp5, which harbors three WW-domains (Figure 6A) (Gupta et al., 2007; Lin et al., 2008; O'Donnell et al., 2013; Becuwe and Leon, 2014). In addition to binding Rsp5, the α-arrestins bind to membrane proteins, thereby bringing the ubiquitin ligase near its membrane client proteins that lack their own $^{L}/_{P}$PxY motifs. Ubiquitination of membrane proteins serves as a signal for their endocytosis, with many of the early-arriving endocytic proteins having ubiquitin-interaction motifs that aid in cargo clustering at endocytic sites (Weinberg and Drubin, 2012). Not only do membrane cargo proteins get ubiquitinated by Rsp5, but many of the α-arrestins themselves are monoubiquitinated by this ubiquitin ligase (Gupta et al., 2007; Lin et al., 2008; Becuwe et al., 2012; O'Donnell et al., 2013; Ho et al., 2017). This mono-ubiquitination is thought to be activating for α-arrestin function, and in some cases is required for α-arrestin recruitment to the membrane (Lin et al., 2008; MacGurn et al., 2011). More recently, a study by MacDonald *et al.* indicates that the monoubiquitination of the adaptor itself can act as an added anchor point for binding to the Rsp5 ubiquitin ligase (MacDonald et al., 2020). We sought to determine if Aly1 and Aly2 required interaction with Rsp5 and/or monoubiquitination to regulate Git1. We used two classes of Aly1 or Aly2 mutants. The first had each of the $^{L}/_{P}$PxY motifs mutated to $^{L}/_{P}$PxA and is called the 'PY-less' mutant. We have shown that PY-less mutants of *ALY*s fail to bind Rsp5, are no longer mono-ubiquitinated and fail to execute all the clathrin-mediated endocytic functions ascribed to date (O'Donnell et al., 2013; Prosser et al., 2015). The second mutant class has the single lysine needed for α-arrestin mono-ubiquitination mutated to arginine. We mapped this monoubiquitination site on Aly1 to lysine 379 and on Aly2 to lysine 392 using mass spectroscopy analyses and demonstrated previously that these K-to-R mutants are no longer ubiquitinated (Hager et al., 2018). We next introduced plasmid-borne versions of each of these mutants into *aly1*Δ *aly2*Δ cells and assessed their GPI sensitivity and Git1 trafficking. In keeping with all earlier observations, the 'PY-less' mutant versions of either Aly1 or Aly2 were completely non-functional in these assays, and so *aly1*Δ *aly2*Δ cells containing Aly1$^{PY\text{-}less}$ or Aly2$^{PY\text{-}less}$ remained sensitive to GPI and the

Git1-GFP PM/vacuole balance remained constant (Figures 6B-D). The Aly1^{K379R} mutant was as resistant to GPI as cells expressing Aly1 and slightly better at inducing steady state or substrate-induced trafficking of Git1 (Figure 6B-D). In contrast, cells with Aly2^{K392R} mutant were more sensitive to GPI than Aly2 cells. The steady-state trafficking of Git1-GFP to the vacuole appeared to be somewhat impaired in cells expressing Aly2^{K392R} but upon GPI addition this mutant reduced PM/vacuole ratios as effectively as Aly2 (Figure 6B-D).

These data demonstrate that while binding of Aly1 and Aly2 to Rsp5 is needed for their function with Git1, monoubiquitination of either of these α-arrestins has only a modest if any impact on their ability to traffic Git1.

Aly1-mediated trafficking of Git1 is modestly regulated by the protein phosphatase calcineurin

Our earlier studies showed that α-arrestin Aly1 binds the protein phosphatase calcineurin (CN) through a canonical 8-amino acid 'PxIxIT' motif, in this case with the sequence PILKIN found in the C-terminal tail of Aly1 (Figure 6A) (O'Donnell et al., 2013). CN is a calcium- and calmodulin-dependent protein phosphatase conserved from yeast to man (Roy and Cyert, 2009, 2020). In humans, CN regulates T-cell differentiation, cardiac function and impacts memory and learning (Klee and Haiech, 1980; Klee and Means, 2002). In yeast, calcineurin helps cells adapt to stressors by regulating the nuclear translocation of the Crz1 transcription factor (Stathopoulos and Cyert, 1997; Cyert, 2003). However, CN also senses and regulates lipid homeostasis; specifically, it helps control sphingolipid balance through its downstream substrates (Bultynck et al., 2006; Tabuchi et al., 2006). Given that GPI transport through Git1 influences PI and sphingolipid levels in cells (Figure 1A), we sought to determine if CN-dependent regulation of Aly1 might influence its role in Git1 trafficking. To do this we made use of mutants that altered CN-regulation of Aly1 in two ways. First, we used Aly1 mutants that lack the CN binding site—either Aly1$^{\Delta PILKIN}$, where the site was deleted, or Aly1^{AAAAAA}, where each residue in this motif was mutated to alanine. In each of these mutants, CN can no longer bind to or dephosphorylate Aly1, and therefore Aly1 is retained in its phosphorylated state (O'Donnell et al., 2013), providing that the kinases needed to phosphorylate Aly1, which remain undefined, are active. Second, from our earlier studies we identified 5 residues—T250, S252, S568, S569, and S573—whose modification was dependent on CN (O'Donnell et al., 2013). Here we use Aly1 mutants where each of these sites was converted to alanine (referred to as Aly1^{5A}), mimicking the dephosphorylated state, or a glutamic acid (referred to as Aly1^{5E}), mimicking the phosphorylated state (O'Donnell et al., 2013). These site mutations bypass the need for kinase activity and directly modulate the CN-regulated sites.

Cells expressing Aly1 or Aly1^{5A} (mimics constitutively dephosphorylated Aly1) gave rise to the strongest restoration of growth on GPI, while the Aly1$^{\Delta PILKIN}$ and Aly1^{AAAAAA} (which cannot be dephosphorylated by CN) gave a slightly more modest rescue of the growth on GPI than wild-type Aly1. Finally, Aly1^{5E} (mimics constitutively phosphorylated Aly1) only marginally improved growth on GPI (Figure 7A). When we examined the localization of Git1 under steady-state conditions, we again find that addition of Aly1 to *aly1*Δ *aly2*Δ cells gave only a modest reduction in the PM/vacuole ratio of Git1 that was not significantly

different from the vector (Suppl. Figure 5A-B). The mutant versions of Aly1 that lack the CN-binding site, Aly1$^{\Delta PILKIN}$ and Aly1^{AAAAAA}, and the CN-regulated phospho-mimetic Aly1^{5E} all failed to significantly alter the PM/vacuole Git1 fluorescence intensities when compared to the vector control (Suppl. Figure 5A-B). It could be the case that under these conditions the kinase responsible for phosphorylating Aly1 is active and therefore retains these mutants as well as the wild-type Aly1 in an inactive state. However, cells containing Aly1^{5A}, which mimics a constitutively dephosphorylated form of Aly1 at these 5 sites, had significantly reduced PM/vacuole ratios compared to *aly1*Δ *aly2*Δ cells with a vector control (Supplemental Figure 5A-B). To better assess Aly1 function under conditions where it would be more active, we next explored GPI-induced trafficking of these same cells and found that when GPI was added Aly1, Aly1$^{\Delta PILKIN}$, Aly1^{AAAAAA}, Aly1^{5A} and Aly1^{5E} all significantly reduced the PM/vacuole fluorescence ratio in comparison to *aly1*Δ *aly2*Δ containing vector alone (Figure 7B-C). However, the Aly1^{5A} mutation that mimics the dephosphorylated form, stimulated vacuolar trafficking of Git1 best in these conditions (Figure 7B-C). Taken together, these data further support a model whereby Aly1 plays a modest role in the steady-state trafficking of Git1, however GPI addition stimulates Aly1's role in Git1 trafficking to the vacuole. Finally, in response to GPI the dephosphorylation mimetic allele, Aly1^{5A}, is best able to traffic Git1 to the vacuole while the phosphorylated mimetic, Aly1^{5E}, modestly rescued growth of *aly1*Δ *aly2*Δ on GPI-containing medium. These results are consistent with CN acting as a modest positive regulator of Aly1-mediated trafficking of Git1.

While these data suggest that CN–acting through Aly1–is a modest positive regulator of Git1 trafficking to the vacuole, we were surprised to see that when we deleted Cnb1, the regulatory subunit of CN, Git1 trafficking to the vacuole was greatly increased (Figure 8A-B). In contrast to the modest effects observed when exploring CN-regulation of Aly1, this dramatic change in steady-state localization of Git1 in the absence of CN function suggests that CN plays a largely inhibitory role on the vacuolar sorting of Git1. We sought to define the genetic relationship between the Alys and CN in controlling Git1 localization. We found that *cnb1*Δ cells were resistance to GPI and trafficked Git1 to the vacuole, which addition of GPI did not alter (Figures 8D-E). Importantly, loss of Aly1 and Aly2 completely blocked the *cnb1*Δ-induced resistance to GPI and prevented Git1 transit to the vacuole (Figure 8D-E), demonstrating that the Aly1/Aly2 regulation of Git1 is epistatic to that of Cnb1.

Aly-dependent alterations in sphingolipid and phosphoinositide metabolism

The GPI internalized via Git1 releases free inositol that is incorporated into PI. Since PI is a precursor to sphingolipid and phosphoinositide production (Figure 1A and Figure 8C), we probed these pathways for alterations when either α-arrestin-mediated or general protein trafficking were perturbed and queried regulation by CN. First, we examined the sensitivity of cells lacking Aly1 and/or Aly2 to myriocin, a drug that inhibits the enzymes Lcb1 and Lcb2 which act in the first step of the *de novo* sphingolipid synthesis pathway (Figure 8C), and aureobasidin, a drug that blocks the phosphatidylinositol:ceramide phosphoinositol transferase Aur1's ability to convert ceramide to inositol phosphorylceramide (IPC) in sphingolipid synthesis (Figure 8C) (Angus and Lester, 1972; Dickson et al., 2006; Epstein et

al., 2012; Klug and Daum, 2014; Montefusco et al., 2014). Since elevated [^{3}H]-GPI uptake leads to higher conversion of the inositol label into PI (Figure 10C) and PI is required for complex sphingolipid biosynthesis, we hypothesized that Aly loss might make cells resistant sphingolipid synthesis inhibitors. However, this is not what we observed. Loss of Aly1 and Aly2 caused modest sensitivity to myriocin and aureobasidin (Figure 8D), that was rescued by addition of phytosphingosine (PHS) (Suppl. Figure 6A), suggestive of defective flux through this pathway (Figure 8C). Other endocytic mutants, including *vrp1*Δ and *end3*Δ, or ESCRT mutants *vps4*Δ and *vsp27*Δ, which each likely increase membrane protein abundance at the PM, similarly showed sensitivity to myriocin that can, in all but *end3*Δ cells, be partially rescued by PHS addition (Suppl. Figure 6A). Given the importance of sphingolipids in the PM and other membranes, it is not surprising that defects in membrane trafficking may change sphingolipid balance. Many trafficking mutants have defects in sphingolipid balance, including the Golgi-associated retrograde protein (GARP) complex (Frohlich et al., 2015), regulators of Niemann-Pick type C disease (Newton et al., 2018), and Rab proteins (Choudhury et al., 2002). Based on these data it appears that the α-arrestins Aly1 and Aly2 influence sphingolipid homeostasis as well, however the linkage to Git1 regulation is unclear.

We next examined *cnb1*Δ cells and found they were resistant to myriocin and sensitive to aureobasidin (Figure 8D), consistent with a role for CN as an effector of sphingolipid biosynthesis (Dunn et al., 1998; Bultynck et al., 2006; Tabuchi et al., 2006; Muir et al., 2014). However, the *aly1*Δ *aly2*Δ *cnb1*Δ cells were wild-type like in their sensitivity to myriocin but completely resistant to aureobasidin, suggesting a more complex interplay between these α-arrestins and CN. Given that CN impinges upon the sphingolipid biosynthesis pathway at multiple points, including i) dephosphorylation of Lac1/Lag1 ii) regulation of Csg2 and iii) dephosphorylation of the Slm proteins (Dunn et al., 1998; Bultynck et al., 2006; Tabuchi et al., 2006; Muir et al., 2014), it is unlikely that the genetic interaction would solely be explained via the α-arrestins. Considering these broad roles in sphingolipid regulation for CN, it is interesting that the *aly1*Δ *aly2*Δ reversed the aureobasidin sensitivity for *cnb1*Δ cells (Figure 8D). To begin to determine if any of these phenotypes were linked to Git1 trafficking, we over-expressed Git1-GFP in each of these mutants and found that this increased resistance to myriocin in all but the *cnb1*Δ cells, while increasing sensitivity to aureobasidin (Figure 8D). This result was not expected since we thought elevated Git1 would increase GPI uptake and PI levels, which should aid in sphingolipid biosynthesis. While these data further define a role for Git1, CN and endocytic trafficking in influencing sphingolipids, the underlying mechanism for these altered sensitivities to sphingolipid inhibition remain to be fully elucidated.

In addition to feeding PI into the sphingolipid biosynthetic pathway, uptake of GPI through Git1 and its subsequent release of inositol could elevate PI to cause changes in membrane phospholipid production. To survey the phospholipid distributions in cells where Aly1 and Aly2 were lost, we examined the localization and abundance of probes for phosphatidylserine (PS, Lact-C2-GFP probe) as well as phosphatidylinositol 4-phosphate (PI(4)P, GFP-2xPH-Osh2 and GFP-P4Mx1 probes), phosphatidylinositol 3-phosphate (PI(3)P, GFP-FYVE-Eea1 probe), and phosphatidylinositol 4,5-bisphosphate (PI(4,5)P_2, GFP-2xPH-Plcδ). We found no significant changes in PI(4)P or PI(4,5)P_2 in the absence

of α-arrestins Aly1 or Aly2 (Suppl. Figure 7A-C). However, there were dramatic changes in PI(3)P and PS in the *aly1*Δ *aly2*Δ mutant compared to wild-type cells (Figure 9A-B and Suppl. Figure 7D-E). Interestingly, the PI(3)P, which typically marks the endosomal compartment in wild-type cells, was significantly brighter and distributed to the limiting membrane of the vacuole in the absence of the Alys. Mutations that disrupt endocytosis and the trafficking of Git1, such as *end3*Δ, *vrp1*Δ and *apl1*Δ, did not result in similar elevations of PI(3)P on the limiting membrane of the vacuole (Figure 9C), though for *end3*Δ there was an issue with the expression of the GFP-Eea1-FYVE probe (Figure 9D). The other mutants examined had equivalent expression of the GFP-Eea1-FYVE to that observed in WT cells (Figure 9D). Though it is somewhat unclear how these specific phospholipid species, and not others, would be influenced by α-arrestins, we sought to determine if alteration of PI(3)P could in any way be linked to GPI uptake through Git1. We treated cells with GPI and monitored GFP-FYVE-Eea1 localization and abundance changes. We found that even in wild-type cells treated with GPI, PI(3)P-associated fluorescence increased with brighter PI(3)P signal on the limiting membrane of the vacuole (Figure 10A-B). In the absence of *ALY1* and *ALY2*, not only did cells start out with more PI(3)P on the vacuolar membrane, but the abundance further increased upon GPI addition (Figure 10A-B). To further assess the linkage between GPI uptake and PI conversion as possibly fueling these changes in phospholipid balance, we provided cells with [^{3}H]-inositol-GPI and monitored the presence of the inositol label across extracellular, soluble intracellular, and membrane fractions (Table 1). These assays were performed using the endogenous Git1 transporter under growth conditions that would allow for *GIT1* expression (see Methods). As shown in Table 1 and Figure 10C, *aly1Δ aly2Δ* cells incorporated a greater percentage of inositol label from exogenous GPI into the cell as both a TCA-extractable (water-soluble) fraction and into a particulate membrane fraction as compared to wild-type cells during the labeling period. Roughly 2.5 times the amount of soluble intracellular inositol label and 4 times as much PI was found in *aly1Δ aly2Δ* as compared to wild-type (Table 1). This result is consistent with increased stability, and hence activity, of Git1 at the PM in *aly1Δ aly2Δ* cells. It is important to note that the labeled metabolites detected, including PI, do not represent total internal pools, but rather represent only those molecules that received inositol label from exogenous [^{3}H]-GPI. In addition to this pool, *de novo* synthesis of inositol will be a major source of unlabeled inositol and that pool is not monitored by these assays (Henry et al., 2012; Henry et al., 2014). These data confirm the known linkage between GPI uptake and incorporation of released inositol into PI and show that the α-arrestins Aly1 and Aly2 play an important role in this regulation (Table 1) (Patton et al., 1995; Patton-Vogt and Henry, 1998; Almaguer et al., 2003; Almaguer et al., 2004). This is not a completely unexpected functional link between GPI uptake, its conversion to PI and an increase in PI(3)P, as these pathways are well-documented. However, our findings do not demonstrate that all of the aberrant PI(3)P accumulation on *aly1*Δ *aly2*Δ vacuoles is due to GPI uptake via Git1. In fact, under the conditions used for the PI(3)P imaging assays we would expect very little Git1 to be at the PM and so there must be additional mechanisms by which *aly1*Δ *aly2*Δ cause elevated PI(3)P that remain to be explored.

Discussion

Our findings demonstrate that α-arrestins Aly1 and Aly2 regulate trafficking of Git1 transporter to the vacuole by regulating its endocytosis and its intracellular sorting (Figure 11). We find that Git1 is internalized in response to the presence of its substrate, GPI, and both basal and substrate-induced internalization are dependent upon the Alys. There is an interesting division of labor between the Alys, with Aly2 controlling Git1 trafficking under steady-state conditions and Aly1 trafficking Git1 in response to GPI. Here we find Git1 internalization depends upon clathrin, consistent with earlier studies (Almaguer et al., 2006), as we can block at least some Git1 endocytosis using mutations in clathrin-coated pit assembly, by preventing actin polymerization using LatA or with mutants lacking the clathrin adaptor complex AP-2. This latter finding is interesting since there are very few endocytic cargos associated with AP-2 in yeast and we have previously found that Alys can each interact directly with AP-2 (O'Donnell et al., 2010). Finally, both Aly1 and Aly2 must interact with the ubiquitin ligase Rsp5 to control Git1 trafficking, though their function is not dramatically hampered by loss of their respective mono-ubiquitination sites.

While endocytosis plays a clear role in Git1 trafficking, intracellular sorting also contributes to Git1 trafficking to the vacuole. Evidence in support of an intracellular sorting mechanism driving Git1 to the vacuole includes the fact that *end3*Δ or LatA-treated cells do not retain as much Git1 at the PM as *aly1*Δ *aly2*Δ cells, suggesting that these α-arrestins help sort Git1 to the vacuole in addition to regulating endocytosis. LatA is effective at blocking the impact of Aly2 on Git1 localization but does not seem as effective at blocking Aly1-mediated trafficking of Git1 to the vacuole. In addition, the block to vacuolar trafficking of Git1 in *aly1*Δ *aly2*Δ cells upon GPI addition is incomplete, suggesting that other adaptors or pathways are also important. Indeed, we find a role for the Buls in altering Git1 protein abundance and trafficking, and this is not the first example of a functional overlap between the Alys and the Buls (Crapeau et al., 2014). Additional α-arrestins may play minor roles in Git1 trafficking since i) *aly1*Δ *aly2*Δ cells are not as effective as 9ArrΔ cells (where the Buls are intact) in retaining endogenous Git1 at the cell surface and ii) in the 9ArrΔ cells, Aly1 is more effective at trafficking Git1 under basal conditions than it is in the *aly1*Δ *aly2*Δ cells, suggesting that it may still be competing with other α-arrestins for access to the cargo in this latter cell type.

α-Arrestin Aly1 is dephosphorylated by the protein phosphatase CN and this activity is needed for optimal Aly1-mediated endocytosis of the aspartic acid permease Dip5 in response to excess substrate (O'Donnell et al., 2013). However, the role of CN-regulation in Git1 trafficking is more complex than this, perhaps due to CN's broader functions in regulating sphingolipid homeostasis. Somewhat surprisingly, mutants of Aly1 that lack the CN-binding site had only a modest impact on Aly1-mediated steady-state or GPI-induced trafficking of Git1, perhaps indicating that the as-yet unknown kinase responsible for countering CN function is not fully active under these conditions. However, a mutant of Aly1 that side-steps the need for kinase function, like the one where the CN-regulated phosphorylation sites were all mutated to alanines to mimic a constitutively dephosphorylated state, significantly improved Git1 trafficking to the vacuole in both

steady-state and substrate-induced conditions. This finding is in keeping with the idea that dephosphorylation improves an α-arrestin's ability to induce trafficking to the vacuole.

It was surprising then to see that loss of the regulatory subunit of CN resulted in robust steady-state trafficking of Git1 to the vacuole, indicating that CN has an inhibitory role in Git1 trafficking. Further, loss of the α-arrestins Aly1 and Aly2 in the *cnb1*Δ strains completely blocked this trafficking, demonstrating that the negative regulation CN exerts on this pathway occurs, either directly or indirectly, via the α-arrestins. Perhaps the altered sensitivities to myriocin and aureobasidin, two drugs that inhibit steps in the sphingolipid biosynthetic pathway, upon Git1 overexpression is linked to this element of CN regulation. Indeed, complex sphingolipid production is reduced under conditions where cells are starved for inositol and/or PI and elevated in conditions where there is excess inositol and/or PI (Henry et al., 2014). When Git1 is retained at the cell surface it should provide added GPI and, subsequent to its breakdown, inositol for PI synthesis. This should then augment sphingolipid production and provide resistance to drugs that impede the pathway (Henry et al., 2012; Henry et al., 2014). However, counter to this anticipated model we find increased sensitivity to aureobasidin when Git1 is overexpressed in cells. The reason for this phenotype is unclear, but it is important to note that these inhibitor studies were performed in the absence of exogenous GPI (Figure 8D) to avoid its toxicity phenotype. Without GPI supplementation, the extracellular levels of GPI available for transport are estimated to be 1–2 μM per OD in a wild-type cell (Angus and Lester, 1972; Patton-Vogt and Henry, 1998) and so may not have a dramatic impact on PI levels. Instead, the observed sensitivity result may be related to a broader role for the Alys in altering trafficking of multiple membrane proteins and/or changing the signaling landscape. In the end, while our data suggest interesting connections between α-arrestins, Git1, CN and sphingolipid balance, the mechanistic links remains to be resolved.

A striking finding from this work is the dramatic alteration in certain phospholipid species associated with loss of the Alys and exacerbated by addition of GPI as monitored through imaging. While PI(3)P is typically sequestered to endosomal membranes, we show a substantial increase in PI(3)P on the limiting membrane of the vacuoles in *aly1*Δ *aly2*Δ cells. Although this phenotype can be linked at least in part to the activity of Git1, since addition of GPI to either wild-type or *aly1*Δ *aly2*Δ cells increased PI(3)P on vacuolar membranes, it seems unlikely that all of the PI(3)P accumulation in the absence of Alys is due solely to Git1. In yeast cells, PI conversion to PI(3)P occurs through the action of Vps34, the phosphatidylinositol 3-kinase (Schu et al., 1993). Perhaps this enrichment in PI(3)P in *aly1*Δ *aly2*Δ cells, which is exacerbated upon GPI addition, is due to hyperactivite Vps34. Conversely, aberrant Fig 4, the PI(3,5)P_2 phosphatase localized to vacuole and nuclear periphery (Gary et al., 2002), or Fab1, the vacuole-localized PI(3)P kinase that generates PI(3,5)P_2, activity may contribute to the elevated PI(3)P. However, given the relatively small pool of PI(3,5)P_2 in cells this seems somewhat less likely (Hasegawa et al., 2017).

Conversion of PI(3)P back into PI is regulated by the PI(3)P phosphatase, Ymr1, and the synaptojanin-like phosphatases, Sjl2 and Sjl3 (Parrish et al., 2004). In mutants lacking Ymr1 and Sjls there is aberrant accumulation of PI(3)P on the limiting membrane of the vacuole and a vacuole fragmentation phenotype (Parrish et al., 2004). While there is no observable

vacuole fragmentation in *aly1*Δ *aly2*Δ, loss of Ymr1/Sjl activity could contribute to the elevated PI(3)P on vacuoles. It will be interesting to see the influence of GPI on the activity of these many PIP regulatory pathways, as it seems feasible that the mechanism by which Git1 retention at the cell surface leads to GPI-induced toxicity could be through alteration of PIP levels. Indeed, maintaining the balance of PIPs in cells is critical as defects in phospholipid metabolism and regulation can be toxic (Strahl and Thorner, 2007; Shyu et al., 2019).

Future studies may reveal a broader role for α-arrestins in contributing to phospholipid balance in cells and help uncover the underlying mechanism behind these phospholipid changes. While many components that disrupt protein trafficking alter phospholipid ratios in the cell, the link here between excess GPI uptake due to Git1 retention at the cell surface, conversion of internalized GPI to PI and specific enrichment of PI(3)P at the vacuolar membrane in the absence of α-arrestins Aly1 and Aly2 represent significant new findings and demonstrate that α-arrestins contribute to phospholipid balance in a previously unanticipated way.

Materials and Methods

Yeast strains and growth conditions

All yeast strains used in this study are derived from the BY4741 genetic background of *S. cerevisiae* (S288C in origin) and are described in detail in Table 2. Yeast were grown in synthetic complete (SC) medium lacking the appropriate nutrient for plasmid maintenance as described in (Johnston et al., 1977) or YPD medium where indicated. Liquid medium was filter sterilized and solid medium for agar plates had 2% agar w/v added before autoclaving. Yeast cells were grown at 30°C unless otherwise noted.

Plasmid and DNA manipulations

Plasmids used in this work are described in Table 3. PCR amplifications for generating plasmid constructs were performed using Phusion High Fidelity DNA Polymerase (ThermoFisher Scientific, Waltham, MA) and sequence insertions were verified using Sanger sequencing (Genewiz, South Plainfield, NJ). Plasmids were transformed into yeast cells using the lithium acetate method (Gietz and Schiestl, 2007) and selected for on the appropriate SC medium lacking the specific nutrient marker.

Serial dilution growth assays

Yeast cells were grown overnight in liquid culture at 30°C in either SC or YPD medium as appropriate. The saturated culture's absorbance at 600 nm (A_{600}) was measured and a starting concentration of A_{600} = 1.0 (which corresponds to approximately 1.0×10^7 cells/ml) was generated. This starting density was diluted in 5-fold series, plated onto the indicated medium and grown for 3–6 days as indicated at 30°C. Plate images were captured on an HP flatbed scanner or using a Chemidoc XRS+ imager (BioRad, Hercules, CA) and all were evenly modified in Photoshop (Adobe Systems Incorporated, San Jose, CA). For GPI containing plates, the GPI was obtained from the Patton-Vogt lab and the final concentration used is indicated in each figure. The myriocin (EMD Millipore, Burlington, MA) and

aureobasidin (Takara Contech, Shiga, Japan) concentrations used are indicated in each figure panel.

Yeast protein extraction and immunoblot analyses

Whole cell extracts of yeast were made using the trichloroacetic acid (TCA) extraction method as previously described (Hager et al., 2018) and as modified from (Volland et al., 1994). Extracts were resolved by SDS-PAGE and proteins were identified using immunoblotting with mouse anti-GFP antibody (Santa Cruz Biotechnology, Santa Cruz, CA) and a rabbit anti-Zwf1 (glucose-6-phosphate dehydrogenase, referred to as G6PDH) antibody (Sigma, St. Louis, MO) as a protein loading control. As an alternative protein loading control, immunoblot membranes were stained after transfer with Revert™ (Li-Cor Biosciences, Lincoln, NE) total protein stain and detected using the Odyssey™ FC infrared imaging system. Anti-mouse or anti-rabbit secondary antibodies conjugated to IRDye-800 or IRDye-680 (Li-Cor Biosciences, Lincoln, NE) were used to detect primary antibodies, visualized on an Odyssey™ FC infrared imaging systems (Li-Cor Biosciences). Quantification of band intensities on immunoblot scans was performed using Image J software (NIH, Bethesda, MD). In brief, each band was boxed, and the mean pixel intensity measured. The background fluorescence was subtracted from each measurement and then the ratio of the GFP-breakdown band over the full-length Git1-GFP band is presented below the immunoblot figures.

Fluorescence microscopy

To assess Git1-GFP or GFP-tagged phospholipid probe localization and/or abundance cells were grown overnight to saturation in SC medium, inoculated into fresh SC medium at an A_{600} of 0.2 and grown at 30°C until they reached mid-log phase (A_{600} = 0.5–0.7). Where indicated, cells were treated with 50 μM glycerophosphoinositol (GPI) for the indicated time prior to imaging. Cells treated with latrunculin A (LatA) (Molecular Probes, Eugene, OR) were incubated with 200 μM LatA or an equivalent volume of the dimethyl sulfoxide (DMSO) vehicle control. To visualize vacuoles, cells were stained with 250 μM Cell Tracker Blue CMAC (7-amino-4-chloromethylcoumarin) dye (Life Technologies, Carlsbad, CA). Cells were then plated onto 35 mm glass bottom microwell dishes that were poly-D-lysine coated (MatTek Corporation, Ashland, MA) and imaged using a Nikon Ti inverted microscope (Nikon, Chiyoda, Tokyo, Japan) outfitted with an Orca Flash 4.0 cMOS camera (Hammamatsu, Bridgewater, NJ) and a 100x objective (numerical aperture, 1.49) or one outfitted with a swept-field confocal scan head, EMCCD camera (iXon3; Andor, Belfast, UK) and a 100x objective (numerical aperture, 1.49). Image acquisition was controlled using NIS-Elements software (Nikon) and all images within an experiment were captured using identical settings. Images were cropped and adjusted equivalently using Photoshop software (Adobe Systems Incorporated).

Image quantification and statistical analyses

For all manual fluorescence quantification analyses, fluorescence intensity was measured using ImageJ software (National Institutes of Health, Bethesda, MD). For cell surface fluorescence quantification, a 2-pixel thick line was hand drawn over the plasma membrane (PM) signal and the mean pixel intensity measured with mean background pixel

intensity subtracted (as described in (O'Donnell et al., 2015)). For vacuolar fluorescence quantification, the vacuole profile was defined by using images captured of cells stained with CMAC dye (Life Technologies) which was then overlaid on the GFP images and the GFP signal within the vacuole mask was measured using ImageJ (NIH). The mean background fluorescence intensity was subtracted for the vacuole measures and each vacuole measure was paired to the corresponding plasma membrane quantification. Prism software (GraphPad Software, San Diego, CA) was then used to perform Kruskal-Wallis statistical analyses with Dunn's post hoc test. In all cases, significant p values from these tests are represented as: *, p value <0.1; **, *p* value <0.01; ***, *p* value <0.001; ns, *p* value >0.1 or in some instances where indicated †††, p value <0.001.

For our automated quantification pipeline, we developed an R program called *CellQuant*. The program detects the plasma membrane of cells using a Gaussian blur and simple threshold on the grayscale GFP image. An adaptive threshold based on the minimum plasma membrane radius is then used on the grayscale CMAC vacuole stain to help identify the vacuoles and constrain their size to features that should be smaller than the cell itself. Cells with no detectable vacuolar region are discarded and the fluorescent signal is measured in the GFP channel. The program further pairs the PM fluorescent output measures with the vacuoles and returns the PM/vacuole fluorescent ratios, which are used extensively in this paper. The source code for this pipeline is available at www.odonnelllab.com and https://github.com/sah129/CellQuant. In addition, the Docker image for the program is hosted on Docker Hub at https://hub.docker.com/r/odonnelllab/cellquant, with command-line installation instructions available on GitHub. There are tutorials that can assist individuals who would like to use this pipeline in setting it up on their own systems and we are happy to help users in applying this approach to their own data sets as well.

Radiolabeled [^{3}H]-GPI transport assays and conversion to [^{3}H]-PI

For assays monitoring endogenous Git1 activity in the presence or absence of α-arrestins, BY4741 and *aly1*Δ *aly2*Δ cells (biological triplicates of each) were grown aerobically overnight at 30°C in yeast nitrogen base (YNB) medium altered to lack inositol and to contain a low level (200μM) of KH_2PO_4 inorganic phosphate and 2% glucose. Amino acid concentrations were as described in (Hanscho et al., 2012). These conditions were needed to allow for robust expression of the endogenous Git1 transporter. The next day, single cultures were used to inoculate two fresh cultures containing either 100μM (low) or 10mM (high) inorganic phosphate at an A_{600} of 0.2. All cultures were allowed to reach an A_{600} of 0.5, at which point they were harvested and assayed for transport activity as described below.

Transport assays to monitor endogenous Git1 transport or *TEF1pr*-Git1-GFP transport of GPI were performed as described in (Surlow et al., 2014). For the Git1-GFP assays, cells were precultured in high phosphate medium only, as described above, as low phosphate medium was not required to induce expression of Git1. Cells were then harvested by filtration, washed with water and resuspended in 100mM citrate buffer [pH 5] to an A_{600} = 5.0. The assays were initiated by adding 50μl of 75μM [^{3}H]-GPI to 200μl of cell suspension. After a 4-minute incubation at 30°C, the assays were stopped by the addition of ice cold distilled, deionized water. Samples were then filtered over Whatman GFC filters

(Whatman number 1822–025), washed with 10ml of ice cold distilled, deionized water, and resuspended in 10 ml of scintillation fluid for radioactivity counts. A Student's t-test was used to assess significance and the data from three biological replicates are shown with each having two technical replicates performed (6 replicates in total). GPI was purchased from Sigma Chemical Company, Tritium labeled GPI ([^{3}H]-inositol-GPI) was produced through the deacylation of phosphatidyl[^{3}H]-myo-inositol purchased from American Radiolabeled Chemicals, as described (Hama et al., 2000).

For assessments of the conversion of GPI to PI after uptake (as in Table 1 and Figure 10C), wild-type or *aly1*Δ *aly2*Δ cultures (biological triplicate) were grown aerobically overnight at 30°C in YNB medium altered to lack inositol and contain a low level of KH_2PO_4 (200μM) and 2% glucose. Amino acid concentrations were as described (Hanscho et al., 2012). The medium lacked inositol (I-) and contained a low KH_2PO_4 level to induce expression of the *GIT1* transporter for GPI uptake. The overnight cultures were diluted to log phase in fresh media containing a high level of KH_2PO_4 (10 mM) and allowed to double. To begin labeling, 4 ml cultures normalized to OD_{600} =0.2 were spiked with 5μM [^{3}H]-GPI (100,00 cpm/ml). The cultures were harvested following aerobic growth at 30°C for 5 hours. A membrane fraction, a TCA-extractable intracellular fraction and an extracellular fraction were isolated as described previously (Surlow et al., 2014). The percentages of radioactive counts in each fraction were determined using a liquid scintillation counter. Lipids were extracted from the membrane fraction and separated by thin layer chromatography as described previously (Surlow et al., 2014). Radioactive (American Radiolabeled Chemicals Inc.) and nonradioactive (Avanti Polar Lipid) phosphatidylinositol (PI) standards were used to verify the migration of PI on the TLC plate. Tritium labeled GPI ([^{3}H]-inositol-GPI) was produced through the deacylation of phosphatidyl[^{3}H]-myo-inositol, as described in (Hama et al., 2000).

Supplementary Material

Refer to Web version on PubMed Central for supplementary material.

Acknowledgements

We thank members of the O'Donnell lab, especially Nejla Ozbaki-Yagan for strain construction, and the Patton-Vogt lab, as well as the Pittsburgh Area Yeast community, for their critical feedback on this work. We thank Dr. Gerry Hammond (Univ. of Pittsburgh) for the PI(4,5)P_2 probe.

Funding

This research was funded by the National Sciences Foundation (MCB CAREER 1902859 and 1553143 to A.F.O.) and the National Institutes of Health (R15 GM 104876 to J.P.V.). The work was also supported by start-up funds from the Depts of Biological Sciences at Duquesne University and the Univ. of Pittsburgh to A.F.O.

Abbreviations

a.u.	arbitrary units
CDP	cytidine diphosphate
DMSO	Dimethyl sulfoxide

GPI	glycerophosphoinositol
LatA	Latrunculin A
PI	phospatidylinositol
PI(3)P	phosphatidylinositol-3-phosphate
PI(4)P	phosphatidylinositol-4-phosphate
PI(3,5)P_2	phosphatidylinositol-3,5-bisphosphate
PI(4,5)P_2	phosphatidylinositol-4,5-bisphosphate
PS	phosphatidylserine

References

Almaguer C, Cheng W, Nolder C, and Patton-Vogt J (2004). Glycerophosphoinositol, a novel phosphate source whose transport is regulated by multiple factors in Saccharomyces cerevisiae. J Biol Chem 279, 31937–31942. [PubMed: 15145930]

Almaguer C, Fisher E, and Patton-Vogt J (2006). Posttranscriptional regulation of Git1p, the glycerophosphoinositol/glycerophosphocholine transporter of Saccharomyces cerevisiae. Curr Genet 50, 367–375. [PubMed: 16924500]

Almaguer C, Mantella D, Perez E, and Patton-Vogt J (2003). Inositol and phosphate regulate GIT1 transcription and glycerophosphoinositol incorporation in Saccharomyces cerevisiae. Eukaryot Cell 2, 729–736. [PubMed: 12912892]

Alvaro CG, O'Donnell AF, Prosser DC, Augustine AA, Goldman A, Brodsky JL, Cyert MS, Wendland B, and Thorner J (2014). Specific alpha-arrestins negatively regulate Saccharomyces cerevisiae pheromone response by down-modulating the G-protein-coupled receptor Ste2. Mol Cell Biol 34, 2660–2681. [PubMed: 24820415]

Angus WW, and Lester RL (1972). Turnover of inositol and phosphorus containing lipids in Saccharomyces cerevisiae; extracellular accumulation of glycerophosphorylinositol derived from phosphatidylinositol. Arch Biochem Biophys 151, 483–495. [PubMed: 4339932]

Ayscough KR, Stryker J, Pokala N, Sanders M, Crews P, and Drubin DG (1997). High rates of actin filament turnover in budding yeast and roles for actin in establishment and maintenance of cell polarity revealed using the actin inhibitor latrunculin-A. J Cell Biol 137, 399–416. [PubMed: 9128251]

Becuwe M, and Leon S (2014). Integrated control of transporter endocytosis and recycling by the arrestin-related protein Rod1 and the ubiquitin ligase Rsp5. Elife 3.

Becuwe M, Vieira N, Lara D, Gomes-Rezende J, Soares-Cunha C, Casal M, Haguenauer-Tsapis R, Vincent O, Paiva S, and Leon S (2012). A molecular switch on an arrestin-like protein relays glucose signaling to transporter endocytosis. J Cell Biol 196, 247–259. [PubMed: 22249293]

Behnia R, and Munro S (2005). Organelle identity and the signposts for membrane traffic. Nature 438, 597–604. [PubMed: 16319879]

Blondel MO, Morvan J, Dupre S, Urban-Grimal D, Haguenauer-Tsapis R, and Volland C (2004). Direct sorting of the yeast uracil permease to the endosomal system is controlled by uracil binding and Rsp5p-dependent ubiquitylation. Mol Biol Cell 15, 883–895. [PubMed: 14657252]

Bultynck G, Heath VL, Majeed AP, Galan JM, Haguenauer-Tsapis R, and Cyert MS (2006). Slm1 and slm2 are novel substrates of the calcineurin phosphatase required for heat stress-induced endocytosis of the yeast uracil permease. Mol Cell Biol 26, 4729–4745. [PubMed: 16738335]

Burd CG, and Emr SD (1998). Phosphatidylinositol(3)-phosphate signaling mediated by specific binding to RING FYVE domains. Mol Cell 2, 157–162. [PubMed: 9702203]

Carroll SY, Stimpson HE, Weinberg J, Toret CP, Sun Y, and Drubin DG (2012). Analysis of yeast endocytic site formation and maturation through a regulatory transition point. Mol Biol Cell 23, 657–668. [PubMed: 22190733]

Carroll SY, Stirling PC, Stimpson HE, Giesselmann E, Schmitt MJ, and Drubin DG (2009). A yeast killer toxin screen provides insights into a/b toxin entry, trafficking, and killing mechanisms. Dev Cell 17, 552–560. [PubMed: 19853568]

Casares D, Escriba PV, and Rossello CA (2019). Membrane Lipid Composition: Effect on Membrane and Organelle Structure, Function and Compartmentalization and Therapeutic Avenues. Int J Mol Sci 20.

Chandrashekarappa DG, McCartney RR, O'Donnell AF, and Schmidt MC (2016). The beta subunit of yeast AMP-activated protein kinase directs substrate specificity in response to alkaline stress. Cell Signal 28, 1881–1893. [PubMed: 27592031]

Choudhury A, Dominguez M, Puri V, Sharma DK, Narita K, Wheatley CL, Marks DL, and Pagano RE (2002). Rab proteins mediate Golgi transport of caveola-internalized glycosphingolipids and correct lipid trafficking in Niemann-Pick C cells. J Clin Invest 109, 1541–1550. [PubMed: 12070301]

Crapeau M, Merhi A, and Andre B (2014). Stress conditions promote yeast Gap1 permease ubiquitylation and down-regulation via the arrestin-like Bul and Aly proteins. J Biol Chem 289, 22103–22116. [PubMed: 24942738]

Cyert MS (2003). Calcineurin signaling in Saccharomyces cerevisiae: how yeast go crazy in response to stress. Biochem Biophys Res Commun 311, 1143–1150. [PubMed: 14623300]

Di Paolo G, and De Camilli P (2006). Phosphoinositides in cell regulation and membrane dynamics. Nature 443, 651–657. [PubMed: 17035995]

Dickson RC, Sumanasekera C, and Lester RL (2006). Functions and metabolism of sphingolipids in Saccharomyces cerevisiae. Prog Lipid Res 45, 447–465. [PubMed: 16730802]

Dunn TM, Haak D, Monaghan E, and Beeler TJ (1998). Synthesis of monohydroxylated inositolphosphorylceramide (IPC-C) in Saccharomyces cerevisiae requires Scs7p, a protein with both a cytochrome b5-like omain and a hydroxylase/desaturase domain. Yeast 14, 311–321. [PubMed: 9559540]

Epstein S, Castillon GA, Qin Y, and Riezman H (2012). An essential function of sphingolipids in yeast cell division. Mol Microbiol 84, 1018–1032. [PubMed: 22616608]

Fisher E, Almaguer C, Holic R, Griac P, and Patton-Vogt J (2005). Glycerophosphocholine-dependent growth requires Gde1p (YPL110c) and Git1p in Saccharomyces cerevisiae. J Biol Chem 280, 36110–36117. [PubMed: 16141200]

Frohlich F, Petit C, Kory N, Christiano R, Hannibal-Bach HK, Graham M, Liu X, Ejsing CS, Farese RV, and Walther TC (2015). The GARP complex is required for cellular sphingolipid homeostasis. Elife 4.

Gary JD, Sato TK, Stefan CJ, Bonangelino CJ, Weisman LS, and Emr SD (2002). Regulation of Fab1 phosphatidylinositol 3-phosphate 5-kinase pathway by Vac7 protein and Fig4, a polyphosphoinositide phosphatase family member. Mol Biol Cell 13, 1238–1251. [PubMed: 11950935]

Ghaddar K, Merhi A, Saliba E, Krammer EM, Prevost M, and Andre B (2014). Substrate-induced ubiquitylation and endocytosis of yeast amino acid permeases. Mol Cell Biol 34, 4447–4463. [PubMed: 25266656]

Gietz RD, and Schiestl RH (2007). High-efficiency yeast transformation using the LiAc/SS carrier DNA/PEG method. Nat Protoc 2, 31–34. [PubMed: 17401334]

Gillooly DJ, Morrow IC, Lindsay M, Gould R, Bryant NJ, Gaullier JM, Parton RG, and Stenmark H (2000). Localization of phosphatidylinositol 3-phosphate in yeast and mammalian cells. EMBO J 19, 4577–4588. [PubMed: 10970851]

Gournas C, Amillis S, Vlanti A, and Diallinas G (2010). Transport-dependent endocytosis and turnover of a uric acid-xanthine permease. Mol Microbiol 75, 246–260. [PubMed: 20002879]

Gournas C, Saliba E, Krammer EM, Barthelemy C, Prevost M, and Andre B (2017). Transition of yeast Can1 transporter to the inward-facing state unveils an alpha-arrestin target sequence promoting its ubiquitylation and endocytosis. Mol Biol Cell 28, 2819–2832. [PubMed: 28814503]

Gupta R, Kus B, Fladd C, Wasmuth J, Tonikian R, Sidhu S, Krogan NJ, Parkinson J, and Rotin D (2007). Ubiquitination screen using protein microarrays for comprehensive identification of Rsp5 substrates in yeast. Mol Syst Biol 3, 116. [PubMed: 17551511]

Hager NA, Krasowski CJ, Mackie TD, Kolb AR, Needham PG, Augustine AA, Dempsey A, Szent-Gyorgyi C, Bruchez MP, Bain DJ, Kwiatkowski AV, O'Donnell AF, and Brodsky JL (2018). Select alpha-arrestins control cell-surface abundance of the mammalian Kir2.1 potassium channel in a yeast model. J Biol Chem 293, 11006–11021. [PubMed: 29784874]

Hama H, Takemoto JY, and DeWald DB (2000). Analysis of phosphoinositides in protein trafficking. Methods 20, 465–473. [PubMed: 10720467]

Hanscho M, Ruckerbauer DE, Chauhan N, Hofbauer HF, Krahulec S, Nidetzky B, Kohlwein SD, Zanghellini J, and Natter K (2012). Nutritional requirements of the BY series of Saccharomyces cerevisiae strains for optimum growth. FEMS Yeast Res 12, 796–808. [PubMed: 22780918]

Harada Y, Tamura Y, and Endo T (2010). Identification of yeast Art5 as a multicopy suppressor for the mitochondrial translocator maintenance protein Tam41. Biochem Biophys Res Commun 392, 228–233. [PubMed: 20074554]

Hasegawa J, Strunk BS, and Weisman LS (2017). PI5P and PI(3,5)P2: Minor, but Essential Phosphoinositides. Cell Struct Funct 42, 49–60. [PubMed: 28302928]

Hatakeyama R, Kamiya M, Takahara T, and Maeda T (2010). Endocytosis of the aspartic acid/glutamic acid transporter Dip5 is triggered by substrate-dependent recruitment of the Rsp5 ubiquitin ligase via the arrestin-like protein Aly2. Mol Cell Biol 30, 5598–5607. [PubMed: 20956561]

Henry SA, Gaspar ML, and Jesch SA (2014). The response to inositol: regulation of glycerolipid metabolism and stress response signaling in yeast. Chem Phys Lipids 180, 23–43. [PubMed: 24418527]

Henry SA, Kohlwein SD, and Carman GM (2012). Metabolism and regulation of glycerolipids in the yeast Saccharomyces cerevisiae. Genetics 190, 317–349. [PubMed: 22345606]

Ho HC, MacGurn JA, and Emr SD (2017). Deubiquitinating enzymes Ubp2 and Ubp15 regulate endocytosis by limiting ubiquitination and degradation of ARTs. Mol Biol Cell 28, 1271–1283. [PubMed: 28298493]

Hovsepian J, Defenouillere Q, Albanese V, Vachova L, Garcia C, Palkova Z, and Leon S (2017). Multilevel regulation of an alpha-arrestin by glucose depletion controls hexose transporter endocytosis. J Cell Biol 216, 1811–1831. [PubMed: 28468835]

Ivashov V, Zimmer J, Schwabl S, Kahlhofer J, Weys S, Gstir R, Jakschitz T, Kremser L, Bonn GK, Lindner H, Huber LA, Leon S, Schmidt O, and Teis D (2020). Complementary alpha-arrestin-ubiquitin ligase complexes control nutrient transporter endocytosis in response to amino acids. Elife 9.

Johnston GC, Pringle JR, and Hartwell LH (1977). Coordination of growth with cell division in the yeast Saccharomyces cerevisiae. Exp Cell Res 105, 79–98. [PubMed: 320023]

Kahlhofer J, Leon S, Teis D, and Schmidt O (2020). The alpha-arrestin family of ubiquitin ligase adaptors links metabolism with selective endocytosis. Biol Cell.

Keener JM, and Babst M (2013). Quality control and substrate-dependent downregulation of the nutrient transporter Fur4. Traffic 14, 412–427. [PubMed: 23305501]

Kim S, Fyrst H, and Saba J (2000). Accumulation of phosphorylated sphingoid long chain bases results in cell growth inhibition in Saccharomyces cerevisiae. Genetics 156, 1519–1529. [PubMed: 11102354]

Klee CB, and Haiech J (1980). Concerted role of calmodulin and calcineurin in calcium regulation. Ann N Y Acad Sci 356, 43–54. [PubMed: 6263160]

Klee CB, and Means AR (2002). Keeping up with calcium: conference on calcium-binding proteins and calcium function in health and disease. EMBO Rep 3, 823–827. [PubMed: 12223462]

Klemm RW, Ejsing CS, Surma MA, Kaiser HJ, Gerl MJ, Sampaio JL, de Robillard Q, Ferguson C, Proszynski TJ, Shevchenko A, and Simons K (2009). Segregation of sphingolipids and sterols during formation of secretory vesicles at the trans-Golgi network. J Cell Biol 185, 601–612. [PubMed: 19433450]

Klug L, and Daum G (2014). Yeast lipid metabolism at a glance. FEMS Yeast Res 14, 369–388. [PubMed: 24520995]

Li Y, Kane T, Tipper C, Spatrick P, and Jenness DD (1999). Yeast mutants affecting possible quality control of plasma membrane proteins. Mol Cell Biol 19, 3588–3599. [PubMed: 10207082]

Lin CH, MacGurn JA, Chu T, Stefan CJ, and Emr SD (2008). Arrestin-related ubiquitin-ligase adaptors regulate endocytosis and protein turnover at the cell surface. Cell 135, 714–725. [PubMed: 18976803]

Ljungdahl PO, and Daignan-Fornier B (2012). Regulation of amino acid, nucleotide, and phosphate metabolism in Saccharomyces cerevisiae. Genetics 190, 885–929. [PubMed: 22419079]

MacDonald C, Shields SB, Williams CA, Winistorfer S, and Piper RC (2020). A Cycle of Ubiquitination Regulates Adaptor Function of the Nedd4-Family Ubiquitin Ligase Rsp5. Curr Biol 30, 465–479 e465. [PubMed: 31956026]

MacGurn JA, Hsu PC, Smolka MB, and Emr SD (2011). TORC1 regulates endocytosis via Npr1-mediated phosphoinhibition of a ubiquitin ligase adaptor. Cell 147, 1104–1117. [PubMed: 22118465]

Magbanua JP, Ogawa N, Harashima S, and Oshima Y (1997). The transcriptional activators of the PHO regulon, Pho4p and Pho2p, interact directly with each other and with components of the basal transcription machinery in Saccharomyces cerevisiae. J Biochem 121, 1182–1189. [PubMed: 9354395]

Mariggio S, Iurisci C, Sebastia J, Patton-Vogt J, and Corda D (2006). Molecular characterization of a glycerophosphoinositol transporter in mammalian cells. FEBS Lett 580, 6789–6796. [PubMed: 17141226]

Montefusco DJ, Matmati N, and Hannun YA (2014). The yeast sphingolipid signaling landscape. Chem Phys Lipids 177, 26–40. [PubMed: 24220500]

Muir A, Ramachandran S, Roelants FM, Timmons G, and Thorner J (2014). TORC2-dependent protein kinase Ypk1 phosphorylates ceramide synthase to stimulate synthesis of complex sphingolipids. Elife 3.

Newton J, Milstien S, and Spiegel S (2018). Niemann-Pick type C disease: The atypical sphingolipidosis. Adv Biol Regul 70, 82–88. [PubMed: 30205942]

Nikko E, and Pelham HR (2009). Arrestin-mediated endocytosis of yeast plasma membrane transporters. Traffic 10, 1856–1867. [PubMed: 19912579]

Nikko E, Sullivan JA, and Pelham HR (2008). Arrestin-like proteins mediate ubiquitination and endocytosis of the yeast metal transporter Smf1. EMBO Rep 9, 1216–1221. [PubMed: 18953286]

Nishimura A, Tanahashi R, and Takagi H (2020). The yeast alpha-arrestin Art3 is a key regulator for arginine-induced endocytosis of the high-affinity proline transporter Put4. Biochem Biophys Res Commun 531, 416–421. [PubMed: 32800549]

Novoselova TV, Zahira K, Rose RS, and Sullivan JA (2012). Bul proteins, a nonredundant, antagonistic family of ubiquitin ligase regulatory proteins. Eukaryot Cell 11, 463–470. [PubMed: 22307975]

O'Donnell AF (2012). The running of the Buls: control of permease trafficking by alpha-arrestins Bul1 and Bul2. Mol Cell Biol 32, 4506–4509. [PubMed: 23028041]

O'Donnell AF, Apffel A, Gardner RG, and Cyert MS (2010). Alpha-arrestins Aly1 and Aly2 regulate intracellular trafficking in response to nutrient signaling. Mol Biol Cell 21, 3552–3566. [PubMed: 20739461]

O'Donnell AF, Huang L, Thorner J, and Cyert MS (2013). A calcineurin-dependent switch controls the trafficking function of alpha-arrestin Aly1/Art6. J Biol Chem 288, 24063–24080. [PubMed: 23824189]

O'Donnell AF, McCartney RR, Chandrashekarappa DG, Zhang BB, Thorner J, and Schmidt MC (2015). 2-Deoxyglucose impairs Saccharomyces cerevisiae growth by stimulating Snf1-regulated and alpha-arrestin-mediated trafficking of hexose transporters 1 and 3. Mol Cell Biol 35, 939–955. [PubMed: 25547292]

O'Donnell AF, and Schmidt MC (2019). AMPK-Mediated Regulation of Alpha-Arrestins and Protein Trafficking. Int J Mol Sci 20.

Parrish WR, Stefan CJ, and Emr SD (2004). Essential role for the myotubularin-related phosphatase Ymr1p and the synaptojanin-like phosphatases Sjl2p and Sjl3p in regulation of phosphatidylinositol 3-phosphate in yeast. Mol Biol Cell 15, 3567–3579. [PubMed: 15169871]

Patton JL, Pessoa-Brandao L, and Henry SA (1995). Production and reutilization of an extracellular phosphatidylinositol catabolite, glycerophosphoinositol, by Saccharomyces cerevisiae. J Bacteriol 177, 3379–3385. [PubMed: 7768846]

Patton-Vogt JL, and Henry SA (1998). GIT1, a gene encoding a novel transporter for glycerophosphoinositol in Saccharomyces cerevisiae. Genetics 149, 1707–1715. [PubMed: 9691030]

Prosser DC, Pannunzio AE, Brodsky JL, Thorner J, Wendland B, and O'Donnell AF (2015). alpha-Arrestins participate in cargo selection for both clathrin-independent and clathrin-mediated endocytosis. J Cell Sci 128, 4220–4234. [PubMed: 26459639]

Raiborg C, Bache KG, Gillooly DJ, Madshus IH, Stang E, and Stenmark H (2002). Hrs sorts ubiquitinated proteins into clathrin-coated microdomains of early endosomes. Nat Cell Biol 4, 394–398. [PubMed: 11988743]

Risinger AL, Cain NE, Chen EJ, and Kaiser CA (2006). Activity-dependent reversible inactivation of the general amino acid permease. Mol Biol Cell 17, 4411–4419. [PubMed: 16885415]

Rotin D, and Kumar S (2009). Physiological functions of the HECT family of ubiquitin ligases. Nat Rev Mol Cell Biol 10, 398–409. [PubMed: 19436320]

Roy J, and Cyert MS (2009). Cracking the phosphatase code: docking interactions determine substrate specificity. Sci Signal 2, re9.

Roy J, and Cyert MS (2020). Identifying New Substrates and Functions for an Old Enzyme: Calcineurin. Cold Spring Harb Perspect Biol 12.

Ruiz SJ, van 't Klooster JS, Bianchi F, and Poolman B (2020). Growth Inhibition by Amino Acids in Saccharomyces cerevisiae. Microorganisms 9.

Savocco J, Nootens S, Afokpa W, Bausart M, Chen X, Villers J, Renard H, Prevost M, Wattiez R, and Morsomme P (2019) Yeast a-arrestin Art2 is the key regulator of ubiquitylation-dependent endocytosis of plasma membrane vitamin B1 transporters. PLoS Biology 17.

Schu PV, Takegawa K, Fry MJ, Stack JH, Waterfield MD, and Emr SD (1993). Phosphatidylinositol 3-kinase encoded by yeast VPS34 gene essential for protein sorting. Science 260, 88–91. [PubMed: 8385367]

Sen A, Hsieh WC, Hanna CB, Hsu CC, Pearson M 2nd, Tao WA, and Aguilar RC (2020). The Na(+) pump Ena1 is a yeast epsin-specific cargo requiring its ubiquitylation and phosphorylation sites for internalization. J Cell Sci 133.

Shao D, Creasy CL, and Bergman LW (1998). A cysteine residue in helixII of the bHLH domain is essential for homodimerization of the yeast transcription factor Pho4p. Nucleic Acids Res 26, 710–714. [PubMed: 9443961]

Shih SC, Sloper-Mould KE, and Hicke L (2000). Monoubiquitin carries a novel internalization signal that is appended to activated receptors. EMBO J 19, 187–198. [PubMed: 10637223]

Shyu P Jr., Ng BSH, Ho N, Chaw R, Seah YL, Marvalim C, and Thibault G (2019). Membrane phospholipid alteration causes chronic ER stress through early degradation of homeostatic ER-resident proteins. Sci Rep 9, 8637. [PubMed: 31201345]

Soncini SR, Chandrashekarappa DG, Augustine DA, Callahan KP, O'Donnell AF, and Schmidt MC (2020). Spontaneous mutations that confer resistance to 2-deoxyglucose act through Hxk2 and Snf1 pathways to regulate gene expression and HXT endocytosis. PLoS Genet 16, e1008484.

Stathopoulos AM, and Cyert MS (1997). Calcineurin acts through the CRZ1/TCN1-encoded transcription factor to regulate gene expression in yeast. Genes Dev 11, 3432–3444. [PubMed: 9407035]

Strahl T, and Thorner J (2007). Synthesis and function of membrane phosphoinositides in budding yeast, Saccharomyces cerevisiae. Biochim Biophys Acta 1771, 353–404. [PubMed: 17382260]

Stringer DK, and Piper RC (2011). A single ubiquitin is sufficient for cargo protein entry into MVBs in the absence of ESCRT ubiquitination. J Cell Biol 192, 229–242. [PubMed: 21242292]

Surlow BA, Cooley BM, Needham PG, Brodsky JL, and Patton-Vogt J (2014). Loss of Ypk1, the yeast homolog to the human serum- and glucocorticoid-induced protein kinase, accelerates phospholipase B1-mediated phosphatidylcholine deacylation. J Biol Chem 289, 31591–31604. [PubMed: 25258318]

Tabuchi M, Audhya A, Parsons AB, Boone C, and Emr SD (2006). The phosphatidylinositol 4,5-biphosphate and TORC2 binding proteins Slm1 and Slm2 function in sphingolipid regulation. Mol Cell Biol 26, 5861–5875. [PubMed: 16847337]

Tamura Y, Harada Y, Nishikawa S, Yamano K, Kamiya M, Shiota T, Kuroda T, Kuge O, Sesaki H, Imai K, Tomii K, and Endo T (2013). Tam41 is a CDP-diacylglycerol synthase required for cardiolipin biosynthesis in mitochondria. Cell Metab 17, 709–718. [PubMed: 23623749]

Vogel K, Horz W, and Hinnen A (1989). The two positively acting regulatory proteins PHO2 and PHO4 physically interact with PHO5 upstream activation regions. Mol Cell Biol 9, 2050–2057. [PubMed: 2664469]

Volland C, Urban-Grimal D, Geraud G, and Haguenauer-Tsapis R (1994). Endocytosis and degradation of the yeast uracil permease under adverse conditions. J Biol Chem 269, 9833–9841. [PubMed: 8144575]

Wawrzycka D, Sadlak J, Maciaszczyk-Dziubinska E, and Wysocki R (2019). Rsp5-dependent endocytosis and degradation of the arsenite transporter Acr3 requires its N-terminal acidic tail as an endocytic sorting signal and arrestin-related ubiquitin-ligase adaptors. Biochim Biophys Acta Biomembr 1861, 916–925. [PubMed: 30776335]

Weinberg J, and Drubin DG (2012). Clathrin-mediated endocytosis in budding yeast. Trends Cell Biol 22, 1–13. [PubMed: 22018597]

Yamagami K, Yamamoto T, Sakai S, Mioka T, Sano T, Igarashi Y, and Tanaka K (2015). Inositol depletion restores vesicle transport in yeast phospholipid flippase mutants. PLoS One 10, e0120108. [PubMed: 25781026]

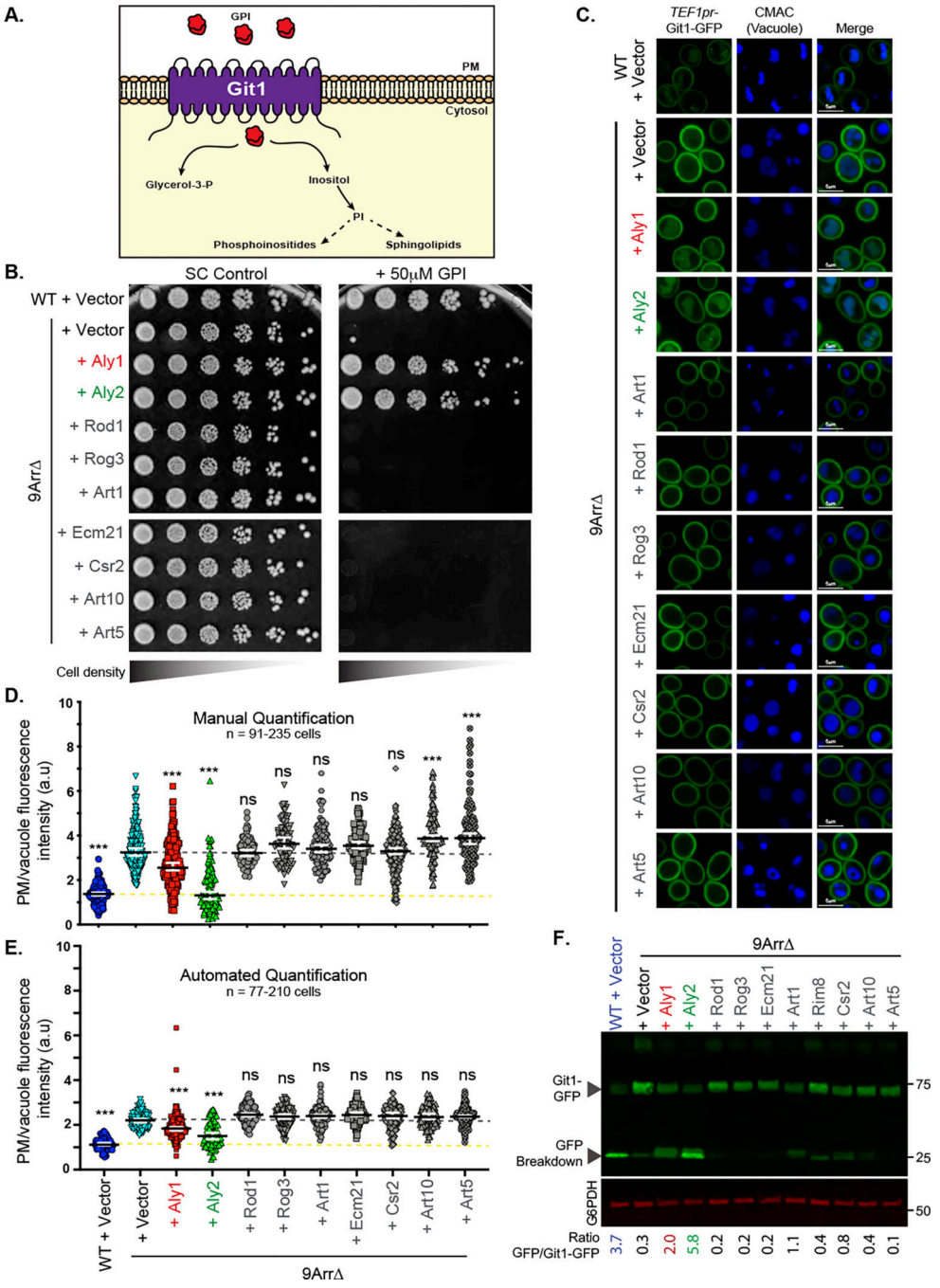

FIGURE 1. Loss of α-arrestins leads to retention of Git1 at the cell surface and sensitivity to GPI.

A, Model of Git1 function at the plasma membrane and influence on downstream metabolic processes. Git1 primarily uptakes GPI, which is then converted to inositol and glycerol-3-phosphate. The inositol can feed into phosphatidylinositol (PI) synthesis, and this influences phosphoinositides and sphingolipids in the cell. *B*, Growth of serial dilutions of WT or 9Arr*Δ* cells all containing a *LEU2*-marked *TEF1pr-GIT1*-GFP plasmid and the indicated pRS316-derived plasmids expressing either nothing (vector) or the indicated α-arrestins on SC medium lacking uracil and leucine and containing 50μM GPI. Growth is shown at 2

days after incubation at 30°C. *C*, WT or 9Arr*Δ* cells containing Git1-GFP expressed from the *TEF1* promoter and either a pRS316 empty vector or plasmid expressing the indicated α-arrestins were imaged by confocal fluorescence microscopy. *D and E*, The PM and vacuolar fluorescence intensities from the cells depicted in C were quantified using either our manual analysis (D) or automated quantification (E) pipelines and the distributions of PM/intracellular fluorescence ratios in arbitrary units (a.u.) were plotted as scatter plots. The horizontal midline in black represents the median and the 95% confidence interval is represented by the white error bars. A yellow dashed line is added as a reference for the median ratio for wild-type cells and the grey dashed line provides a reference for the median value for the 9*Arr*Δ cells. Kruskal-Wallis statistical analyses with Dunn's post hoc test were performed, and statistical significance compared to the *9Arr*Δ strain containing vector control is presented. *F*, Whole cell extracts from cells expressing Git1-GFP and α-arrestin-containing plasmids were analyzed by SDS-PAGE and immunoblotting. Git1-GFP and the GFP-breakdown product abundance is assessed with an anti-GFP antibody and the anti-Zwf1 (G6PDH) antibody is used as a loading control. The ratio of the signal intensities of the GFP breakdown product to the full-length Git-GFP is presented below each lane. Molecular weights of standards are shown at right measured in kilodaltons.

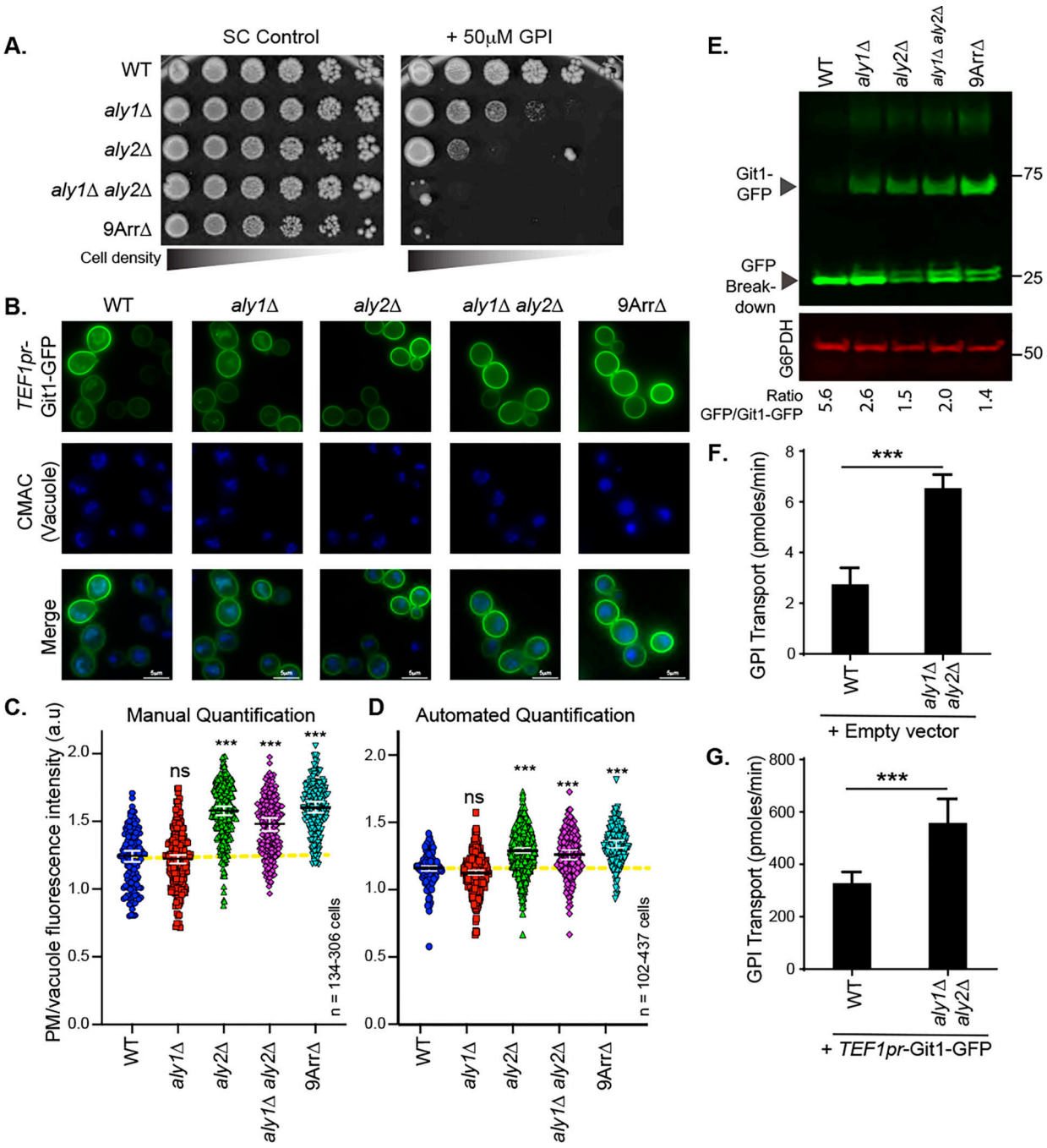

FIGURE 2. Aly1 and Aly2 regulate Git1 localization at the cell surface and loss of these α-arrestins causes GPI sensitivity.

A, Growth of serial dilutions of WT, *aly1Δ, aly2Δ, aly1Δ aly2Δ*, or *9ArrΔ* cells containing the *TEF1pr-GIT1*-GFP plasmid on SC medium lacking leucine and containing 50μM GPI. Growth is shown at 2 days after incubation at 30°C. *B*, The indicated cells containing Git1-GFP expressed from the *TEF1* promoter were stained with CMAC and imaged by fluorescence microscopy. *C and D*, The PM and vacuolar fluorescence intensities from the cells depicted in B were quantified using either our manual (C) or automated quantification (D) pipelines and the distributions of PM/vacuolar fluorescence ratios in arbitrary units

(a.u.) were plotted as scatter plots. The horizontal midline in black represents the median and the 95% confidence interval is represented by the white error bars. A yellow dashed line is added as a reference for the median ratio for wild-type cells. Kruskal-Wallis statistical analyses with Dunn's post hoc test were performed, and statistical significance compared to the wild-type cells is presented. *E*, Whole cell extracts from the indicated cells containing Git1-GFP expressed from the *TEF1* promoter were resolved by SDS-PAGE and immunoblotted with an anti-GFP antibody (to detect Git1-GFP and the GFP breakdown product) and anti-Zwf1 antibody (G6PDH) as a loading control. The ratio of the signal intensities of the GFP breakdown product to the full-length Git-GFP is presented below each lane. Molecular weights of standards are shown at right measured in kilodaltons. *F and G,* GPI radio-labelled uptake assays were performed as described in Surlow et. al., 2014. WT and *aly1Δ aly2Δ* cells containing a *LEU2*-marked *TEF1pr*-GFP empty vector (*F)* or a *LEU2*-marked *TEF1pr-GIT1*-GFP plasmid *(G)* were grown at 30ºC to logarithmic phase and shifted into synthetic media lacking inositol and choline and containing 10mM inorganic phosphate. 50μL of 25μM of [^{3}H]GPI *(F)* or 75μM of [^{3}H]GPI *(G)* was added to 200μL of processed cell suspension. The suspension was then filtered and washed before resuspendion in 10mL of scintillation fluid for counting. Statistical t-test value represents means ± SD of biological triplicates performed in duplicate (6 replicates in total).

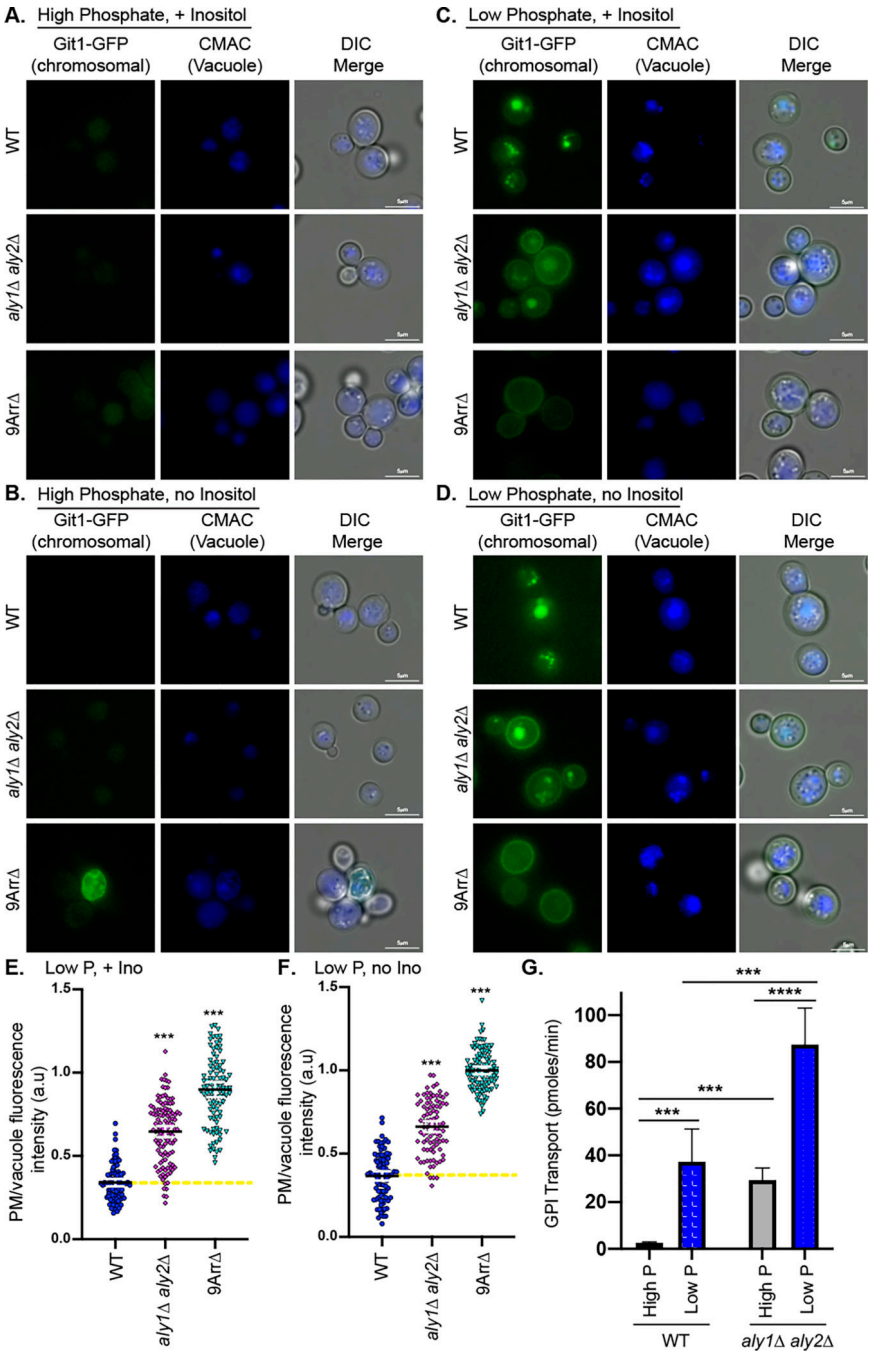

FIGURE 3. Aly1 and Aly2 regulate endogenous Git1 transporter localization and function.

A-D, The indicated cells containing a chromosomally integrated Git1-GFP at its endogenous locus were grown in medium containing high (10mM) or low (100μM) phosphate with or without inositol for 12 h, stained with CMAC and imaged using a fluorescence microscope. *E and F*, The images presented in panels C and D were quantified using our manual quantification methodology and the distributions of PM/ vacuolar fluorescence ratios in arbitrary units (a.u.) were plotted as scatter plots. The horizontal midline in black represents the median and the 95% confidence interval is represented by the white error bars. A

yellow dashed line is added as a reference for the median ratio for wild-type cells. Kruskal-Wallis statistical analyses with Dunn's post hoc test were performed and statistical significance compared to wild-type cells is presented. *G*, GPI radio-labelled uptake assays were performed as described in Surlow et al., 2014. WT and *aly1Δ aly2Δ* cells were grown at 30ºC to logarithmic phase and shifted into synthetic media lacking inositol and choline and containing 100μM (low) or 10mM (high) inorganic phosphate. [^{3}H]GPI was added to 200μL of processed cell suspension for 5 min and cells were filtered and washed before resuspending in 10mL of scintillation fluid for counting. Statistical t-test value represents means ± SD of biological triplicates performed in duplicate (6 replicates in total).

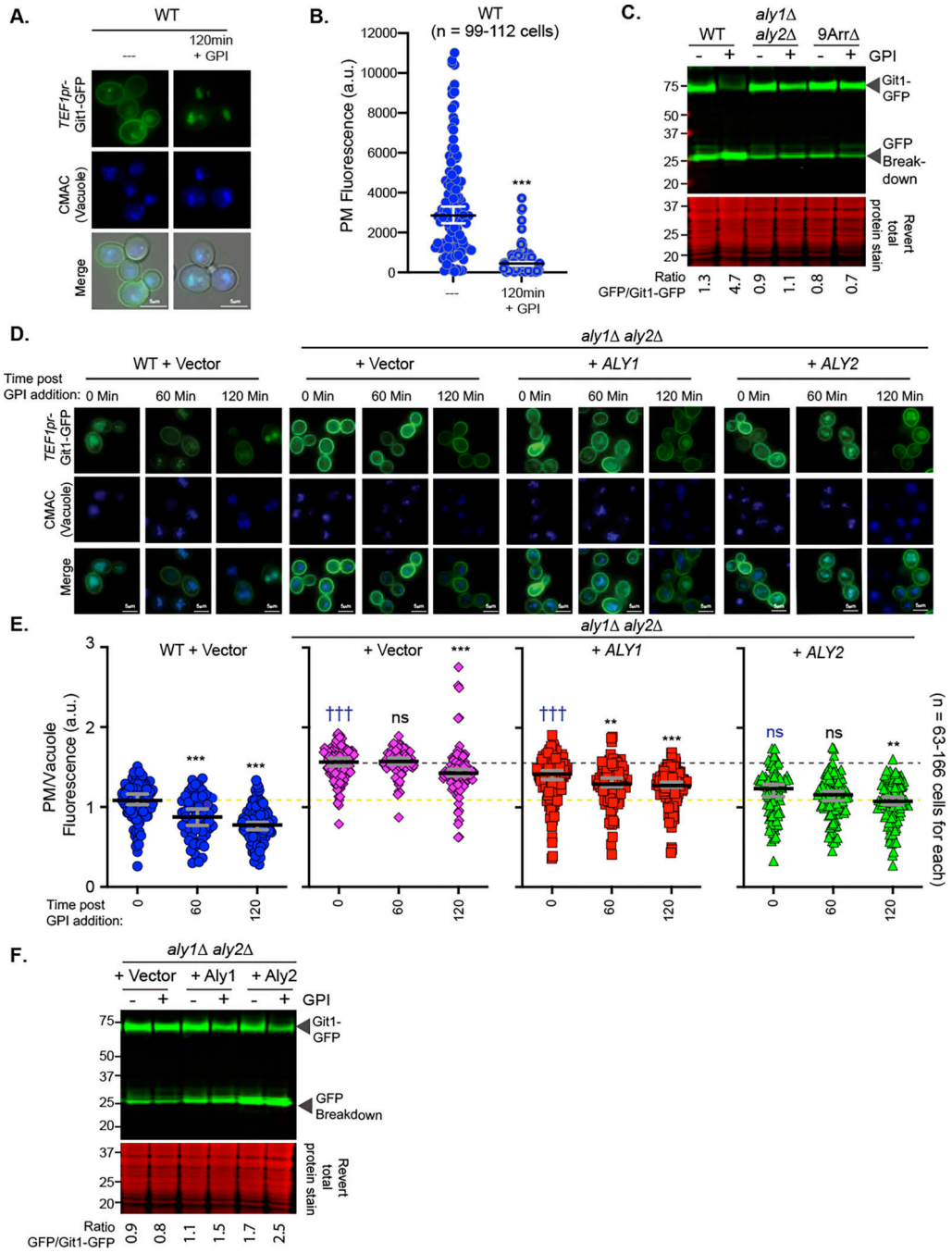

FIGURE 4. Git1 trafficking to the vacuole is induced by GPI addition and Aly1 and Aly2 regulate Git1 sorting to the vacuole.

A, WT cells containing Git1-GFP expressed from the TEF1 promoter were grown in SC medium lacking leucine and then either untreated (---) or incubated with 50μm GPI for 2 hours and imaged by fluorescence microscopy. *B*, Cells in A were manually quantified and the fluorescence intensity at the plasma membrane is reported in arbitrary units. The horizontal midline in black represents the median and the 95% confidence interval is represented by the grey error bars. A Mann-Whitney statistical test was used assess the difference between these two datasets. *C*, Whole cell extracts from untreated cells or those

incubated with GPI for 2h and containing Git1-GFP expressed from the *TEF1* promoter were resolved by SDS-PAGE and immunoblotted with an anti-GFP antibody and Revert total protein stain of the transfer membrane was used as a loading control. The ratio of the signal intensities of the GFP breakdown product to the full-length Git-GFP is presented below each lane. Molecular weights of standards are shown at left measured in kilodaltons. *D,* WT or *aly1Δ aly2Δ* cells containing Git1-GFP expressed from the *TEF1* promoter and either an empty pRS316 vector or one expressing the indicated α-arrestin were cultured in SC media lacking uracil and leucine and containing 50μM GPI for the times indicated before being imaged by fluorescence microscopy. *E,* The PM and vacuolar fluorescence intensities from the cells depicted in A were quantified using our manual quantification pipeline and the distributions of PM/vacuolar fluorescence ratios in arbitrary units (a.u.) were plotted as scatter plots. The horizontal midline in black represents the median and the 95% confidence interval is represented by the grey error bars. Kruskal-Wallis statistical analyses with Dunn's post hoc test were performed, and statistical significance compared to the 0 min point for each graph is presented as asterisks (*) or indicated as not significant (ns). Additionally, the 0 min point for each of the strains is compared back to the wild-type with vector control and these are presented in blue text as daggers (†) or indicated as not significant (ns) where applicable. A yellow dashed line is presented to facilitate comparisons to the WT with vector control at the t=0 min point, and a grey dashed line is presented to facilitate comparisons to the *aly1*Δ *aly2*Δ mutant with vector at the t=0 min point. *F,* Whole cell extracts from untreated cells or those incubated with GPI for 2h and containing Git1-GFP expressed from the *TEF1* promoter were resolved by SDS-PAGE and immunoblotted with an anti-GFP antibody and Revert total protein stain of the transfer membrane was used as a loading control. The ratio of the signal intensities of the GFP breakdown product to the full-length Git-GFP is presented below each lane. Molecular weights of standards are shown at left measured in kilodaltons.

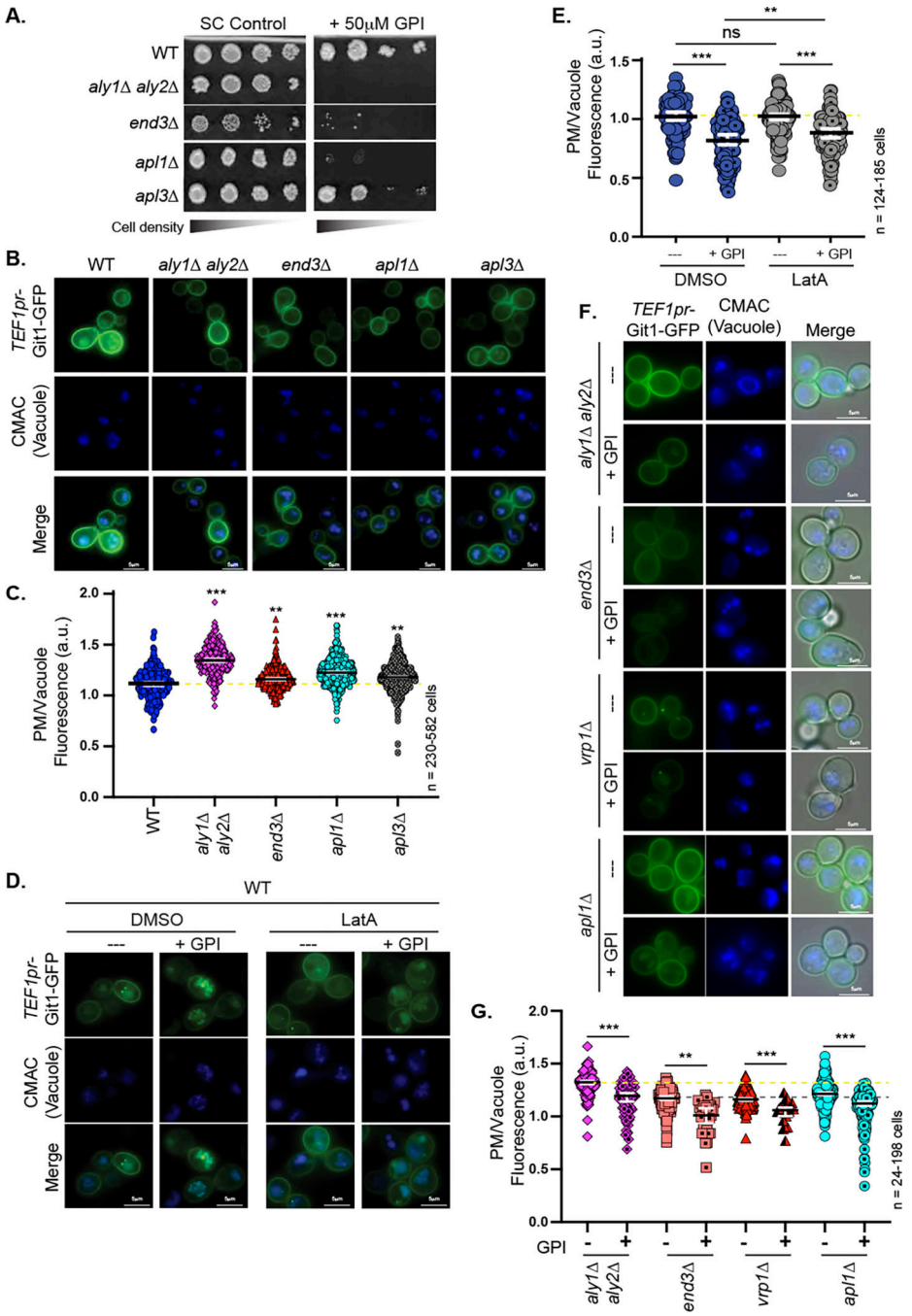

FIGURE 5. GPI induces clathrin-dependent endocytosis of Git1.

A, Growth on SC medium lacking leucine with or without 50μM GPI for serial dilutions of cells from the indicated yeast strains containing a *LEU2*-marked *TEF1pr-GIT1*-GFP plasmid is shown 2 days post-incubation at 30°C. *B,* The indicated cells expressing Git1-GFP from the *TEF1* promoter were stained with CMAC and imaged by fluorescence microscopy. *C, E* and *G,* The PM and vacuolar fluorescence intensities from the cells depicted in B, D or F, respectively, were quantified using our automated quantification pipeline and the distributions of PM/intracellular fluorescence ratios in arbitrary units (a.u.)

were plotted as scatter plots. The horizontal midline in black represents the median and the 95% confidence interval is represented by the white error bars. A yellow dashed line represents the median ratio for untreated wild-type (in C and E) or *aly1*Δ *aly2*Δ (in G) cells to facilitate comparisons. Kruskal-Wallis statistical analyses with Dunn's post hoc test were performed and statistical significance is indicated with asterisks. In panel C, all statistical comparisons indicated are relative to the WT control. *D,* WT cells containing Git1-GFP expressed from the *TEF1* promoter were cultured in SC media lacking leucine and containing 200μM latrunculin A or an equal volume of DMSO for 120 min prior either addition of 50μM GPI or no treatment, and incubated for 120 min further before being stained with CMAC and imaged by fluorescence microscopy. *E,* Cells containing Git1-GFP expressed from the *TEF1* promoter were cultured in SC media lacking leucine and containing 50μM GPI (+ GPI) or no treatment (---) and incubated for 120 min before staining with CMAC and fluorescence microscopy imaging.

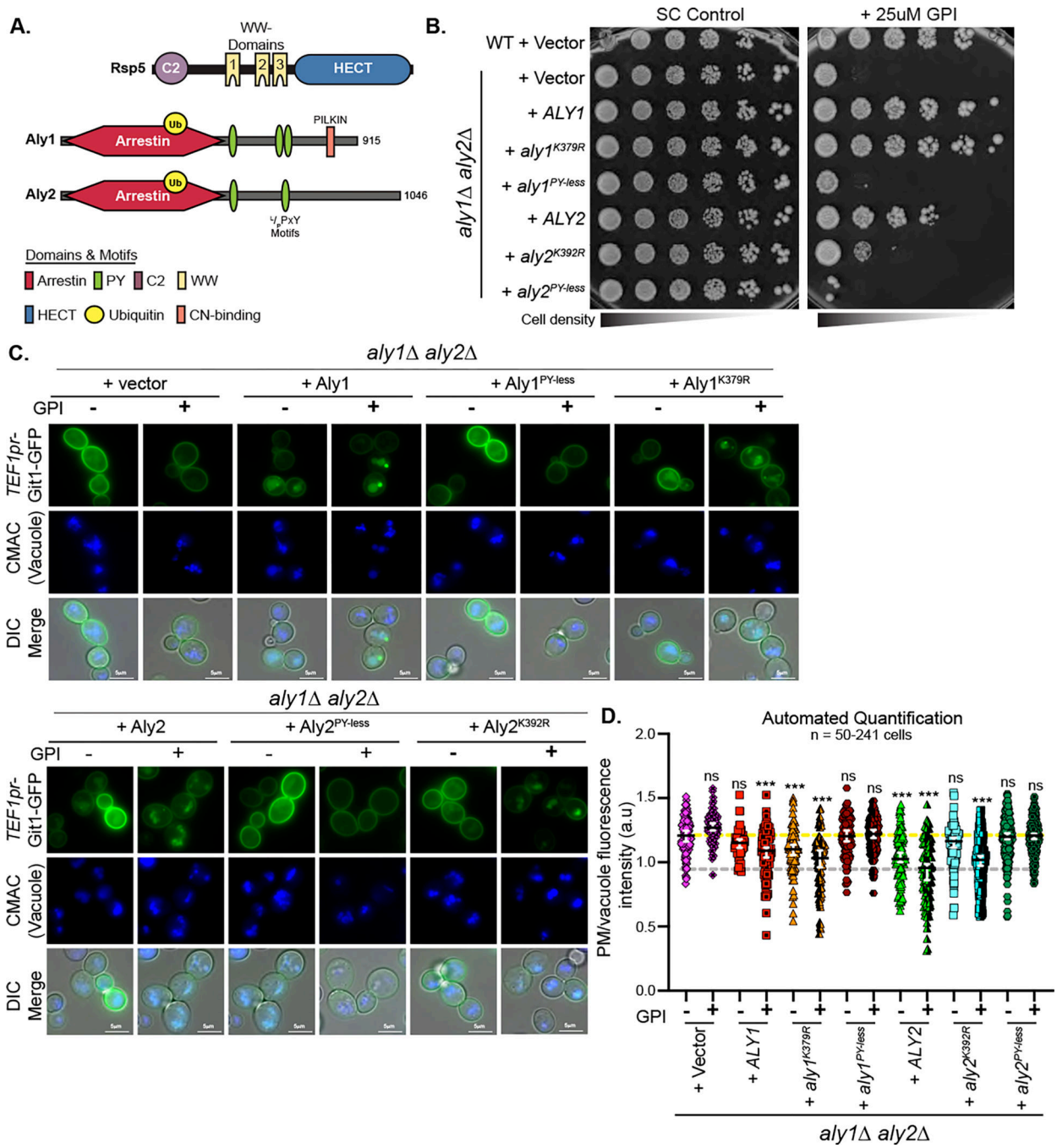

FIGURE 6. Aly1- and Aly2-mediated trafficking of Git1 requires interaction with Rsp5.

A, Schematic of Rsp5 and Aly1/Aly2 domain and motif architecture. The site of monoubiquitination on Aly1 and Aly2 is indicated as a yellow circle. *B*, Growth of serial dilutions of WT or *aly1Δ aly2Δ* cells containing a *LEU2*-marked *TEF1pr-GIT1*-GFP plasmid and plasmids expressing the indicated α-arrestin variant on SC medium lacking uracil and leucine and containing 25μM GPI is presented. Growth is shown after 2 days of incubation at 30°C. *C*, WT or *aly1Δ aly2Δ* cells containing Git1-GFP expressed from the *TEF1* promoter and either an empty pRS316 vector or expressing the indicated α-arrestin

cultured in SC media lacking leucine and containing 50μM GPI (+ GPI) or no treatment (---), and incubated for 120 min before staining with CMAC and fluorescence microscopy imaging. *D*, The PM and vacuolar fluorescence intensities from the cells depicted in C were quantified using our automated quantification pipeline and the distributions of PM/vacuolar fluorescence ratios in arbitrary units (a.u.) were plotted as scatter plots. The horizontal midline in black represents the median and the 95% confidence interval is represented by the white error bars. Kruskal-Wallis statistical analyses with Dunn's post hoc test were performed and statistical significance compared to untreated *aly1*Δ *aly2*Δ cells with vector is indicated with asterisks or as not significant (ns) where applicable. A yellow dashed line that represents the median of the untreated *aly1*Δ *aly2*Δ cells containing a vector control and a grey dashed line that represents the median of *aly1*Δ *aly2*Δ + Aly2 cells treated with GPI is provided to facilitate comparisons.

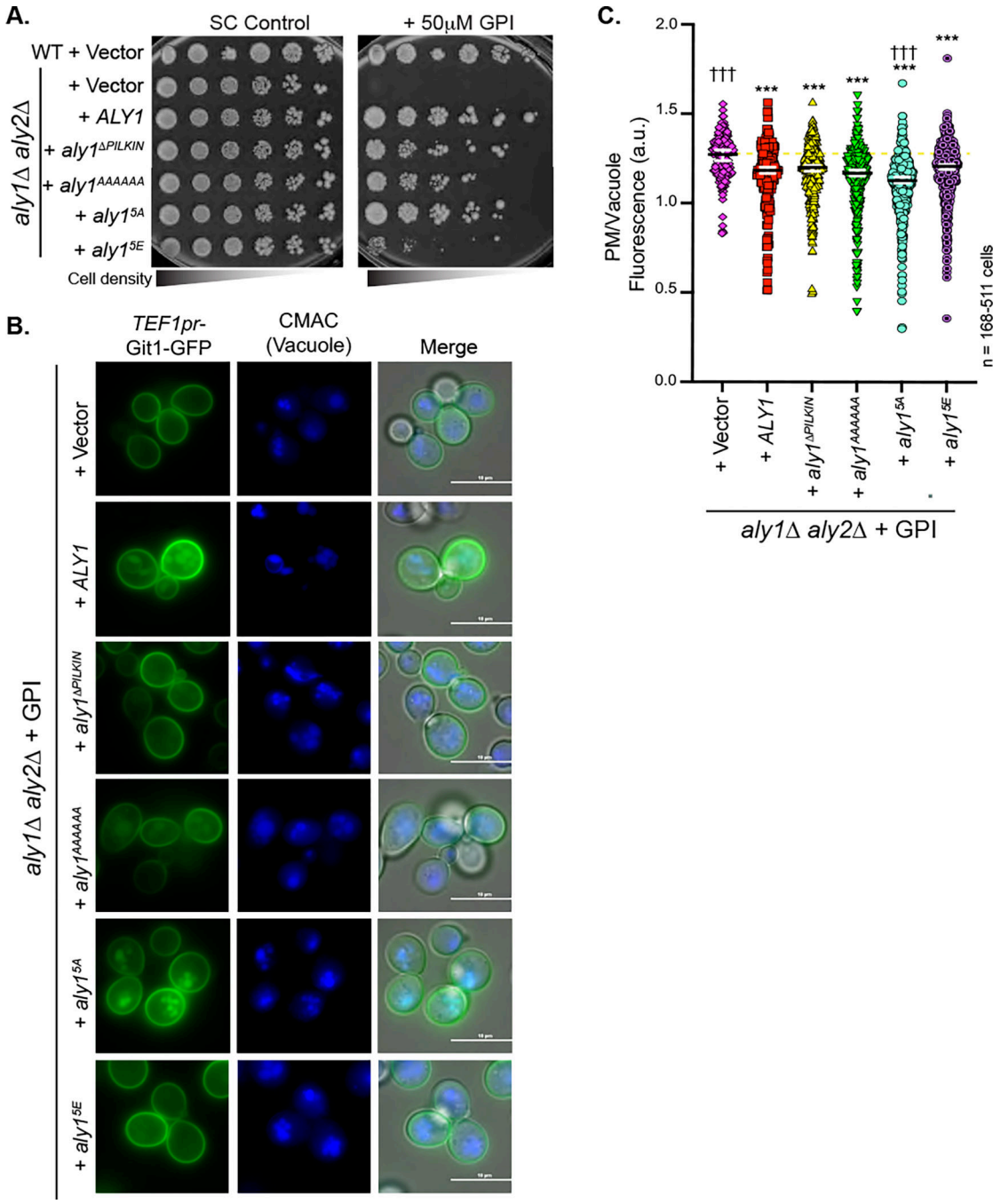

FIGURE 7. Calcineurin-mediated regulation of Aly1 plays a modest role in Git1 trafficking.

A, Growth of serial dilutions of WT or *aly1Δ aly2Δ* cells containing a *LEU2*-marked *TEF1pr-GIT1*-GFP plasmid and an empty pRS316 vector or one expressing the indicated α-arrestins on SC medium lacking uracil and leucine and containing 50μM GPI is shown after 2 days of incubation at 30°C. *B*, Cells lacking *ALY1* and *ALY2* with a plasmid expressing Git1-GFP from the *TEF1* promoter and an empty pRS316 vector or one expressing the indicated α-arrestins were treated with 50μM GPI for 2 h, stained with CMAC and imaged by fluorescence microscopy. *C*, The PM and vacuolar fluorescence intensities from the

cells depicted in *B* were quantified using our automated quantification pipeline and the distributions of PM/intracellular fluorescence ratios in arbitrary units (a.u.) were plotted as scatter plots. The horizontal midline in black represents the median and the 95% confidence interval is represented by the white error bars. Kruskal-Wallis statistical analyses with Dunn's post hoc test were performed and statistical significance compared to the *aly1*Δ *aly2*Δ cells with vector is indicated with asterisks or as not significant (ns) where applicable. The ††† symbols represent p-values of <0.001 and is used to mark comparisons between *aly1*Δ *aly2*Δ expressing *ALY1* and each of the other conditions. In these conditions, most mutants are not statistically different from wild-type Aly1 (no marker shown); Aly1^{5A} is the only mutant that has significantly lower PM/vacuole ratios than wild-type Aly1 while the vector control has significantly higher PM/vacuole ratios. In each case, a yellow dashed line is provided that represents the median of the *aly1*Δ *aly2*Δ cells containing a vector control to facilitate comparisons.

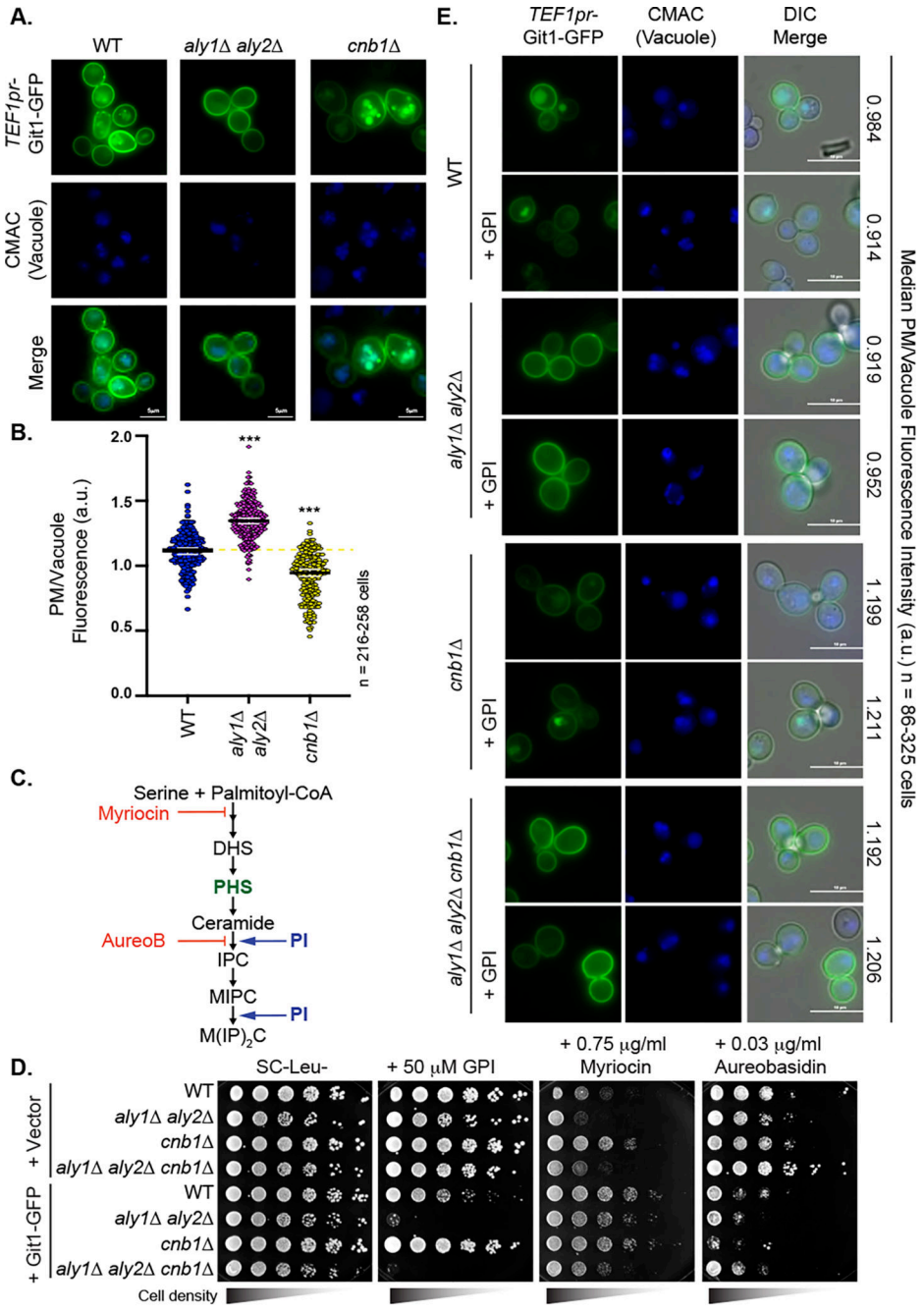

FIGURE 8. Loss of CN increases Git1 trafficking to the vacuole, but *aly1Δ aly2Δ* is epistatic to CN regulation.

A, WT, *aly1Δ aly2Δ*, or *cnb1*Δ cells containing Git1-GFP expressed from the *TEF1* promoter were stained with CMAC and imaged by fluorescence microscopy. *B*, The PM and vacuolar fluorescence intensities from the cells depicted in A were quantified using our automated quantification pipeline and the distributions of PM/vacuolar fluorescence ratios in arbitrary units (a.u.) were plotted as scatter plots. The horizontal midline in black represents the median and the 95% confidence interval is represented by the white error bars. Kruskal-Wallis statistical analyses with Dunn's post hoc test were

performed and statistical significance compared to the wild-type cells is indicated with asterisks. A yellow dashed line is provided that represents the median of wild-type cells to facilitate comparisons. *C,* Schematic of the sphingolipid biosynthetic pathway demonstrating the points where myriocin and aureobasidin (AureoB) impair the pathway (red lines) and the sites where PI is incorporated into the complex base production in the lower half of the pathway (PI with blue arrows). The intermediates in the pathway are shown but the enzymes are not indicated. Abbreviations in this diagram are as follows: DHS (dihydrosphingosine), PHS (phytosphingosine), IPC (inositolphosphoryl-ceramide), MIPIC (mannosylinositolphosphoryl-ceramide), and $M(IP)_2C$ (mannosyl-di-inositolphosphoryl ceramide). For simplicity, some intermediates are not shown and instead, multiple arrowheads are provided for those steps where two or more enzymatic steps have been condensed. *D*, Growth of serial dilutions of the cells indicated containing either a vector or a *LEU2*-marked *TEF1pr-GIT1*-GFP plasmid on SC medium lacking leucine and containing the indicated concentrations of GPI, myriocin, or aureobasidin are shown after 2–4 days of incubation at 30°C. *E*, WT, *aly1Δ aly2Δ*, *cnb1*Δ, or *aly1Δ aly2Δ cnb1*Δ cells containing Git1-GFP expressed from the *TEF1* promoter were treated with 50μM GPI for 2h, stained with CMAC and imaged by fluorescence microscopy. Automated quantification of the PM and vacuole fluorescence intensities was performed and the median PM/vacuole fluorescence intensity for each is presented in arbitrary units (a.u.) on the right side of the figure.

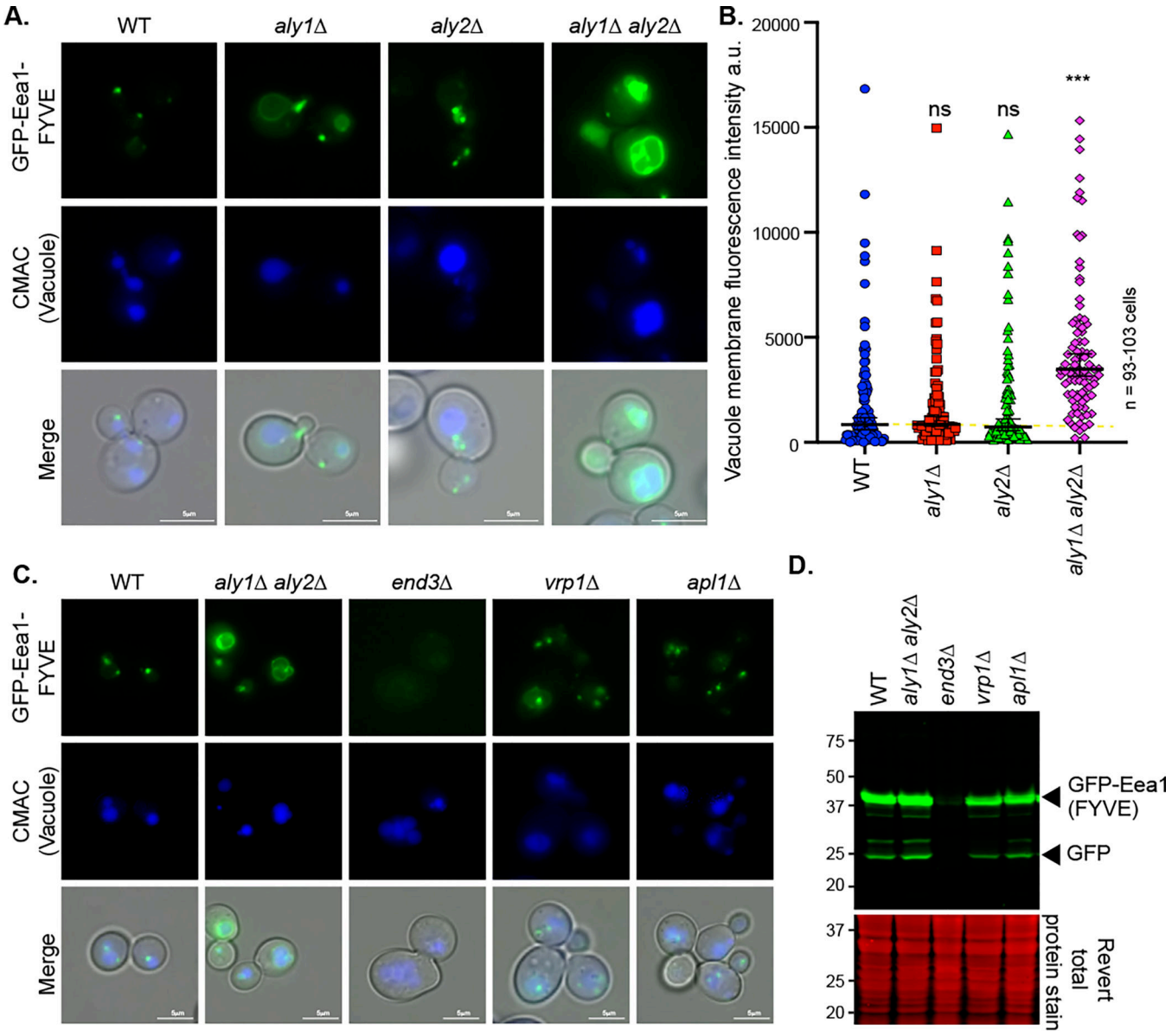

FIGURE 9. Loss of Aly1 and Aly2 disrupts phospholipid balance in the endomembrane system.

A, The indicated cells were transformed with the plasmid expressing a GFP-fused FYVE domain of Eea1, which marks PI(3)P. Cells were stained with CMAC and imaged by fluorescence microscopy. *B*, The GFP fluorescence at the limiting membrane of the vacuole from the images in A was quantified by manually drawing a line around the outside of the CMAC stained vacuoles and overlaying this mask onto the GFP channel. The quantified fluorescence intensities (arbitrary units, a.u.) are presented as scatter plots. The horizontal midline in black represents the median and the 95% confidence interval is represented by the black error bars. Kruskal-Wallis statistical analyses with Dunn's post hoc test were performed and statistical significance compared to the wild-type cells is indicated with asterisks or as not significant (ns) where applicable. A yellow dashed line is provided that represents the median of wild-type cells to facilitate comparisons. *C*, The indicated cells

were transformed with the plasmid expressing a GFP-fused FYVE domain of Eea1, which marks PI(3)P. Cells were stained with CMAC and imaged by fluorescence microscopy. *D*, Whole cell extracts from cells expressing the GFP-fused FYVE domain of Eea1 were resolved by SDS-PAGE and immunoblotted with an anti-GFP antibody and Revert total protein stain of the transfer membrane was used as a loading control. Molecular weights of standards are shown at left measured in kilodaltons.

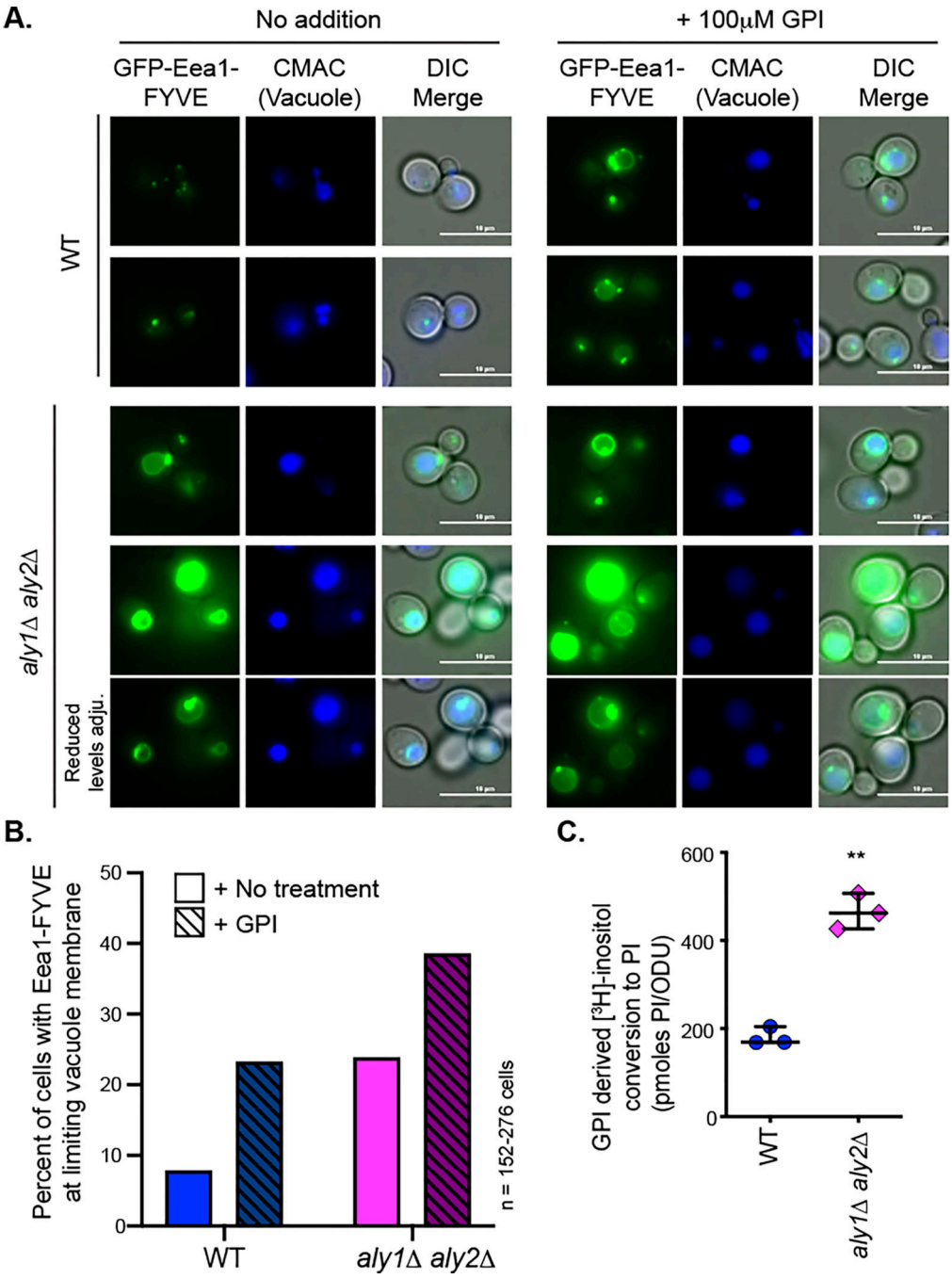

FIGURE 10. GPI uptake is converted into PI and increases PI3P at the limiting membrane of the vacuole.

A, The indicated cells were transformed with the plasmid expressing a GFP-fused FYVE domain of Eea1, which marks PI(3)P. Cells were grown to mid-log phase and either untreated (no addition) or treated with 100μM GPI for 2 h, stained with CMAC and imaged by fluorescence microscopy. *B*, Images of cells captured in A were evenly adjusted. Cells with evident GFP staining of vacuolar limiting membrane were counted in comparison to the total number of vacuoles in the image, as assessed using the CMAC stain. The percentage of cells with limiting membrane fluorescence is presented for each treatment. All cells in

at least 3 images per condition were counted for an n = 150 at minimum per condition. *C*, Radiolabeled [^{3}H]-GPI uptake via the endogenous Git1 transporter and conversion to [^{3}H]-PI was measured in wild-type or *aly1*Δ *aly2*Δ cells. Cells were grown under low phosphate conditions to induce *GIT1* expression in the presence of 5 μM [^{3}H-inositol]-GPI, and intracellular and membrane fractions were isolated. The conversion of [^{3}H]-GPI into [^{3}H]-PI was monitored by using TLC and liquid scintillation counting. The graph presented represents three independent biological replicates that were measured and a Student's t-test was used to assess significance. A more detailed breakdown of these results is presented in Table 1 where both the water-soluble and membrane fractions are compared.

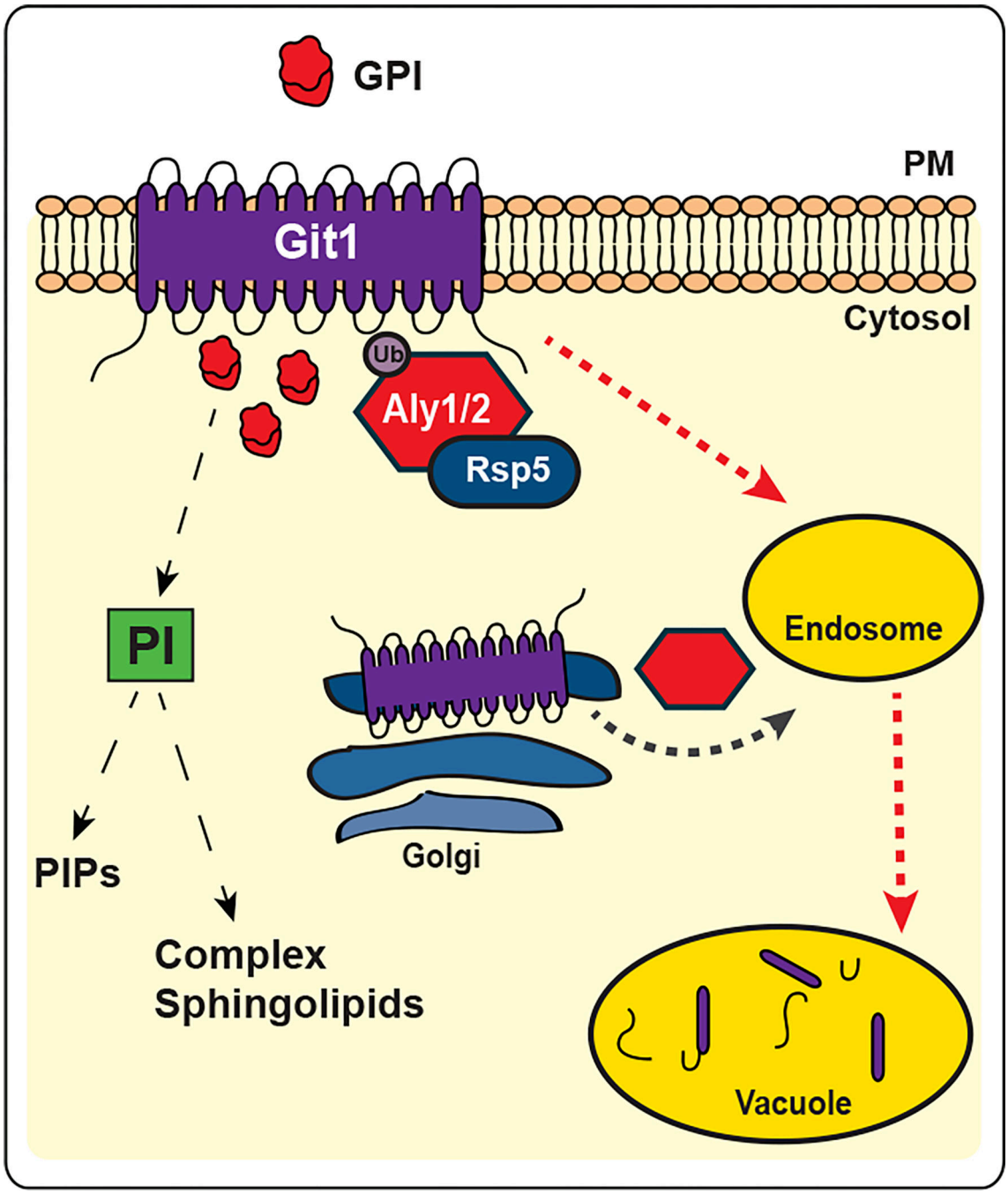

FIGURE 11: Model of α-arrestin regulation of Git1 trafficking.

α-Arrestins are responsible for trafficking of Git1 to the vacuole during both steady-state conditions, where Aly2 is predominantly active, and in response to its substrate GPI, where Aly1 seems to play a more important role. Additionally, an intracellular sorting pathway that is independent of endocytosis contributes to Git1 trafficking to the vacuole and this pathway is also α-arrestin dependent (indicated by grey dashed arrow). Association with the ubiquitin ligase Rsp5 is required for α-arrestin-mediated trafficking of Git1. The endocytic pathway (indicated by red dashed lines) appears to be clathrin-dependent as disruption

of clathrin-associated factors, like End3 and AP-2, leads to retention of Git1 at the cell surface. Uptake of GPI via Git1 may alter the sphingolipid balance in cells and seems to directly influence the distribution of membrane phospholipids, including elevating PI3P on the vacuolar membrane.

Table 1.

Uptake and conversion of [^{3}H]-GPI into [^{3}H]-PI.

Strains were grown in the presence of 5μM [^{3}H-inositol]-GPI (see Methods) and then extracellular, intracellular and membrane fractions were isolated. Lipids were extracted from the membrane fraction and resolved by TLC as described in Methods. The average (Ave.) and standard deviation (St.Dev.) of three individual cultures (biological triplicates) are presented. It should be noted that this experiment was repeated with label of lower specific activity and similar results were obtained.

		Extracellular			Intracellular			Membrane		
Strain	**Rep.**	**%**	**Ave.**	**St.Dev.**	**%**	**Ave.**	**St.Dev.**	**%**	**Ave.**	**St.Dev.**
WT	1	74.73%	**76.34%**	1.40%	18.53%	**17.48%**	1.28%	6.74%	**6.61%**	0.12%
	2	77.03%			16.44%			6.53%		
	3	77.25%			16.20%			6.55%		
aly1Δ aly2Δ	1	35.34%	**31.98%**	3.91%	42.95%	**44.06%**	1.79%	21.71%	**23.96%**	2.24%
	2	27.69%			46.12%			26.19%		
	3	32.90%			43.11%			23.98%		

Table 2.

Yeast Strains

Strain	Genotype	Reference or source
BY4741	*MAT***a***his3Δ1 leu2Δ0 LYS2 met15Δ0 ura3Δ0*	Open Biosystems (Winzeler *et al.*, 1999)
EN60 (9ArrΔ)	*ecm21Δ::KanMX csr2Δ::KanMX bsd2Δ rog3Δ::NatMX rod1Δ ygr068cΔ aly1Δ aly2Δ ylr392cΔ::HIS3 his3Δ0 ura3Δ0 leu2Δ0*	(Nikko and Pelham, 2009)
*aly1*Δ	*MAT***a***his3Δ1 leu2Δ0 LYS2 met15Δ0 ura3Δ0 aly1Δ::KanMX4*	Open Biosystems (Winzeler *et al.*, 1999)
*aly2*Δ	*MAT***a***his3Δ1 leu2Δ0 LYS2 met15Δ0 ura3Δ0 aly2Δ::KanMX4*	Open Biosystems (Winzeler *et al.*, 1999)
*aly1*Δ *aly2*Δ (alias D2–6A)	*MAT***a***his3Δ1 leu2Δ0 MET15 lys2Δ0 ura3Δ0 aly1Δ::KanMX4 aly2Δ::KanMX4*	(O'Donnell et al., 2010)
*end3*Δ	*MAT***a***his3Δ1 leu2Δ0 LYS2 met15Δ0 ura3Δ0 end3Δ::KanMX4*	Gift from D. Prosser
*apl1*Δ	*MAT***a***his3Δ1 leu2Δ0 LYS2 met15Δ0 ura3Δ0 apl1Δ::KanMX4*	Open Biosystems (Winzeler *et al.*, 1999)
*apl3*Δ	*MAT***a***his3Δ1 leu2Δ0 LYS2 met15Δ0 ura3Δ0 apl3Δ::KanMX4*	Open Biosystems (Winzeler *et al.*, 1999)
*cnb1*Δ	*MAT***a***his3Δ1 leu2Δ0 LYS2 met15Δ0 ura3Δ0 cnb1Δ::KanMX4*	Open Biosystems (Winzeler *et al.*, 1999)
*bul1*Δ *bul2*Δ	*MAT***a***his3Δ1 leu2Δ0 MET15 LYS2 ura3Δ0 bul1Δ::KanMX4 bul2Δ::KanMX4*	(O'Donnell et al., 2010)
*bul1*Δ	*MAT***a***his3Δ1 leu2Δ0 LYS2 met15Δ0 ura3Δ0 bul1Δ::KanMX4*	Open Biosystems (Winzeler *et al.*, 1999)
*bul2*Δ	*MAT***a***his3Δ1 leu2Δ0 LYS2 met15Δ0 ura3Δ0 bul2Δ::KanMX4*	Open Biosystems (Winzeler *et al.*, 1999)
*bul1*Δ *aly1*Δ *aly2*Δ	*MAT*α *his3Δ1 leu2Δ0 LYS2 met15Δ0 ura3Δ0 bul1Δ::KanMX4 aly1Δ::NatMX4 aly2Δ::URA3*	(O'Donnell et al., 2010)
*bul2*Δ *aly1*Δ *aly2*Δ	*MAT*α *his3Δ1 leu2Δ0 LYS2 met15Δ0 ura3Δ0 bul2Δ::KanMX4 aly1Δ::NatMX4 aly2Δ::URA3*	(O'Donnell et al., 2010)
*bul1*Δ *bul2*Δ *aly1*Δ *aly2*Δ	*MAT*α *his3Δ1 leu2Δ0 LYS2 met15Δ0 ura3Δ0 bul1Δ::KanMX4 bul2Δ::KanMX4 aly1Δ::NatMX4 aly2Δ::URA3*	(O'Donnell et al., 2010)
*cnb1*Δ	*MAT***a***his3Δ1 leu2Δ0 LYS2 met15Δ0 ura3Δ0 cnb1Δ::HphMX4*	This study
*cnb1*Δ *aly1*Δ *aly2*Δ	*MAT***a***his3Δ1 leu2Δ0 MET15 lys2Δ0 ura3Δ0 aly1Δ::KanMX4 aly2Δ::KanMX4 cnb1Δ::HphMX4*	This study
*vrp1*Δ	*MAT***a***his3Δ1 leu2Δ0 LYS2 met15Δ0 ura3Δ0 vrp1Δ::KanMX4*	Open Biosystems (Winzeler *et al.*, 1999)
*vps4*Δ	*MAT***a***his3Δ1 leu2Δ0 LYS2 met15Δ0 ura3Δ0 vps4Δ::KanMX4*	Open Biosystems (Winzeler *et al.*, 1999)
*vps27*Δ	*MAT***a***his3Δ1 leu2Δ0 LYS2 met15Δ0 ura3Δ0 vps27Δ::KanMX4*	Open Biosystems (Winzeler *et al.*, 1999)
BY4741 Git1-GFP	*MAT***a***GIT1*-GFP::*LEU2 his3Δ1 leu2Δ0 LYS2 met15Δ0 ura3Δ0*	This study
*aly1*Δ *aly2*Δ Git1-GFP	*MAT***a***GIT1*-GFP::*LEU2 his3Δ1 leu2Δ0 MET15 lys2Δ0 ura3Δ0 aly1Δ::KanMX4 aly2Δ::KanMX4*	This study

Table 3.

Plasmids

Name	Description	Reference or source
pRS415-*TEF1pr-GIT1*-GFP	The Git1 coding region, lacking its stop codon, was PCR amplified with primers containing restriction enzyme adaptor sites and cloned into SpeI and HindIII sites of pRS415-*TEF1pr* (described in (Mumberg *et al.*, 1995)) and fused in frame at the C-terminus to eGFP. Between Git1 and eGFP there is a 5 amino acid linker (Ala-Gly-Ala-Gly-Ala-Gly). CEN *LEU2*	This study
pRS316	CEN *URA3*	(Sikorski and Hieter, 1989)
pRS316-Aly1	Genomic clone of *ALY1* expressed from its own promoter; CEN *URA3*	(O'Donnell et al., 2010)
pRS316-Aly2	Genomic clone of *ALY2* expressed from its own promoter; CEN *URA3*	(O'Donnell et al., 2010)
pRS316-Art5	Genomic clone of *ART5* expressed from its own promoter; CEN *URA3*	(O'Donnell et al., 2015)
pRS316-Ldb19	Genomic clone of *LDB19* expressed from its own promoter; CEN *URA3*	(O'Donnell et al., 2015)
pRS316-Art10	Genomic clone of *ART10* expressed from its own promoter; CEN *URA3*	(O'Donnell et al., 2015)
pRS316-Csr2	Genomic clone of *CSR2* expressed from its own promoter; CEN *URA3*	(O'Donnell et al., 2015)
pRS316-Ecm21	Genomic clone of *ECM21* expressed from its own promoter; CEN *URA3*	(O'Donnell et al., 2015)
pRS316-Rod1	Genomic clone of *ROD1* expressed from its own promoter; CEN *URA3*	(O'Donnell et al., 2015)
pRS316-Rog3	Genomic clone of *Rog3* expressed from its own promoter; CEN *URA3*	(O'Donnell et al., 2015)
pRS316-Aly1^{K379R}	This construct was subcloned by digesting the inserted *ALY1* promoter and coding sequence from pRS426-Aly1^{K379R} described in (Hager et al., 2018) and ligating it into pRS316. CEN *URA3*	This study.
pRS316-Aly1^{PPxYless}	This construct was subcloned by digesting the inserted *ALY1* promoter and coding sequence from pRS426-Aly1^{PPxYless} described in (Prosser et al., 2015) and ligating it into pRS316. CEN *URA3*	This study.
pRS316-Aly2^{K392R}	This construct was subcloned by digesting the inserted *ALY2* promoter and coding sequence from pRS426-Aly2^{K392R} described in (Hager et al., 2018) and ligating it into pRS316. CEN *URA3*	This study.
pRS316-Aly2^{PPxYless}	This construct was subcloned by digesting the inserted *ALY2* promoter and coding sequence from pRS426-Aly2^{PPxYless} described in (Prosser et al., 2015) and ligating it into pRS316. CEN *URA3*	This study.
pRS316-Aly1$^{\Delta PILKIN}$	This construct was subcloned by digesting the inserted *ALY1* promoter and coding sequence from pRS426-Aly1$^{\Delta PILKIN}$ (O'Donnell et al., 2013) and ligating it into pRS316. CEN *URA3*	This study.
pRS316-Aly1^{AAAAAA}	This construct was subcloned by digesting the inserted *ALY1* promoter and coding sequence from pRS426-Aly1^{AAAAAA} (O'Donnell et al., 2013) and ligating it into pRS316. CEN *URA3*	This study.
pRS316-Aly1^{5A}	This construct was subcloned by digesting the inserted *ALY1* promoter and coding sequence from pRS426-Aly1^{5A} (O'Donnell et al., 2013) and ligating it into pRS316. CEN *URA3*	This study.
pRS316-Aly1^{5E}	This construct was subcloned by digesting the inserted *ALY1* promoter and coding sequence from pRS426-Aly1^{5E} (O'Donnell et al., 2013) and ligating it into pRS316. CEN *URA3*	This study.

Name	Description	Reference or source
p416-Lact-C2-GFP	Plasmid expresses C2 domain of Lact protein, which recognizes PS, fused to GFP.	Addgene plasmid #22853 (Yeung *et al.*, 2008)
pRS426-GFP-2xPH(Plcδ)	Plasmid expresses 2 tandem copies of the PH domain of Plcδ protein, which recognizes PI(4,5)P2, fused to GFP.	Addgene plasmid #36092 (Stefan *et al.*, 2002)
pRS426-GFP-FYVE(Eea1)	Subcloned from pRS424-GFP-FYVE(Eea1) from Addgene plasmid #36096 (Burd and Emr, 1998) into pRS426. Plasmid expresses the FYVE domain from Eea1, which recognizes PI(3)P, fused to GFP.	This study
pRS426-GFP-2xPH(Osh2)	Subcloned from pRS424-GFP-2xPH(Osh2) from Addgene plasmid #36095 (Stefan *et al.*, 2011)into pRS426. Plasmid expresses two tandem copies of the PH domain from Osh2, which bind to PI(4)P, fused to GFP.	This study
pRS416-GFP-P4Mx1	Subcloned from NES-EGFP-P4Mx1 (Addgene plasmid 108121) into pRS416 for expression in yeast. This plasmid uses the P4Mx1 to detect PI(4)P in cells	(Hammond *et al.*, 2014)